



POLITECNICO DI MILANO
POLO REGIONALE DI LECCO
INDUSTRIAL ENGINEERING FACULTY
MSc. in MECHANICAL ENGINEERING

Temperature Analyses of a Cross Flow Mixing Jet

Graduation Thesis of Yusuf Emin ZEREN - 763077

Supervisor: Professor Aldo COGHE

Academic Year 2011 – 2012

I would like to thank the people who helped me prepare this work and who supported me during this journey.

Thanks to my family and friends in Turkey and Italy.

*Special thanks to **Professor Aldo COGHE** who has always been solicitous and helpful to me during this study.*

Yusuf Emin ZEREN

14/09/2012

TABLE OF CONTENTS

SYMBOL LIST.....	4
FIGURE LIST.....	5
TABLE LIST.....	8
ABSTRACT.....	9
1. INTRODUCTION.....	10
2. LITERATURE REVIEW.....	12
2.1 General View.....	12
2.2 Previous Works.....	13
2.3 Theoretical Development.....	16
2.4 Different Kind of Trajectories.....	17
2.4.1 Two-Dimensional Trajectory.....	17
2.4.2 Three-Dimensional Trajectory.....	20
2.5 Temperature Measurements.....	23
3. TEMPERATURE MEASUREMENTS WITH THERMOCOUPLES	24
3.1 Comparison Of Temperature Measurement Sensors.....	25
3.2 Advantages and Disadvantages of Each Sensor.....	26
3.3 Thermocouples.....	28
3.3.1 Working Principle of Thermocouples.....	29
3.4 Thermocouple Circuits.....	31
3.4.1 Cold-Junction Compensation (CJC).....	31
3.4.2 Software Compensation.....	33
3.4.3 Hardware Compensation.....	33
3.4.4 Voltage To Temperature Conversion.....	34
3.5 Types of Thermocouples.....	37
3.6 Error Estimation.....	40

3.6.1 CJC Errors.....	40
3.6.2 Offset end Gain Errors.....	41
3.6.3 Noise Errors.....	41
3.6.4 Thermocouple Errors.....	42
4. EXPERIMENTAL METHOD.....	43
4.1 Experimental Setup.....	43
4.2 Experimental Apparatus.....	44
4.3 Experimental Procedure.....	47
4.3.1 Correction Procedure.....	48
4.3.2 Thermocouple Positioning.....	49
4.3.3 Calibration of Thermocouple.....	50
5. ANALYSIS AND RESULTS OF THE EXPERIMENTS.....	52
5.1 Analysis of Data for Ratio 1.97	52
5.2 Analysis of Data for Ratio 2.95.....	58
5.3 Analysis of Data for Ratio 4.95.....	64
5.4 Standard Deviation.....	70
6. CONCLUSION.....	72
REFERENCES.....	73

SYMBOL LIST

$N_{Fr,i}$: Froude number of jet flow at injection point

u, w : direction cosines, $\cos \alpha$ and $\cos \beta$, respectively

Δs : infinitesimal length of jet control volume

α, β, γ : inclination of jet axis with respect to X-, Y-, and Z-axis, respectively.

x, y, z : Cartesian (inertial) coordinate system

ρ : average density of jet fluid

ρ_∞ : average density of free-stream fluid

S : Seebeck coefficient

d : effective jet diameter

d_i : diameter of jet orifice

Subscripts:

s, n, t : conditions in s-, n-, and t-direction, respectively

i : conditions at point of jet injection

FIGURE LIST

Figure 2.1	Diagram of the interaction resulting from jet injection into a cross flow.	13
Figure 2.2	Cartesian and natural coordinate system.....	17
Figure 2.3	Experimental and Theoretical Trajectories of an Air Jet.....	18
Figure 2.4	Experimental and Theoretical Trajectories of an Air Jet With Respect to Velocity Ratio.....	19
Figure 2.5	Effect of Froude Number on Jet Trajectory.....	21
Figure 2.6	Effect of Froude Number on Variation of Jet Trajectory Parameters with distance along trajectory for $V_i/V_\infty = 4$, $\alpha_i=90^\circ$ and $\beta_i=45^\circ$	22
Figure 3.1	Temperature measurement sensors.....	25
Figure 3.2	Seebeck Effect.....	29
Figure 3.3	J- Type Thermocouple.....	30
Figure 3.4	Traditional Temperature Measurement with Reference Junction Held at 0°C	31
Figure 3.5	Thermocouple Law of Intermediate Metals.....	32
Figure 3.6	Hardware Compensation Circuit.....	34
Figure 3.7	Thermocouple temperature vs. voltage graph.....	35
Figure 3.8	Seebeck coefficient vs. temperature.....	36
Figure 4.1	Schematic diagram of the duct and transverse jet injection system.....	43
Figure 4.2	Coordinate system.....	43
Figure 4.3	Air Mixing Apparatus.....	45
Figure 4.4	Control Valves and Manometers	46
Figure 4.5	Controller of the Laser Doppler System and Computer.....	47
Figure 4.6	Calibration Curve.....	51
Figure 5.1	3-D plot at first level for ratio 1.97.....	52
Figure 5.2	Contour plot at first level for ratio 1.97.....	53

Figure 5.3	3-D plot at second level for ratio 1.97.....	54
Figure 5.4	Contour plot at second level for ratio 1.97.....	54
Figure 5.5	3-D plot at third level for ratio 1.97.....	55
Figure 5.6	Contour plot at third level for ratio 1.97.....	55
Figure 5.7	3-D plot at fourth level for ratio 1.97.....	56
Figure 5.8	Contour plot at fourth level for ratio 1.97.....	56
Figure 5.9	3-D plot at final level for ratio 1.97.....	57
Figure 5.10	Contour plot at final level for ratio 1.97.....	57
Figure 5.11	3-D plot at first level for ratio 2.95.....	58
Figure 5.12	Contour plot at first level for ratio 2.95.....	59
Figure 5.13	3-D plot at second level for ratio 2.95.....	60
Figure 5.14	Contour plot at second level for ratio 2.95.....	60
Figure 5.15	3-D plot at third level for ratio 2.95.....	61
Figure 5.16	Contour plot at third level for ratio 2.95.....	61
Figure 5.17	3-D plot at fourth level for ratio 2.95.....	62
Figure 5.18	Contour plot at fourth level for ratio 2.95.....	62
Figure 5.19	3-D plot at final level for ratio 2.95.....	63
Figure 5.20	Contour plot at final level for ratio 2.95.....	64
Figure 5.21	3-D plot at first level for ratio 4.95.....	65
Figure 5.22	Counterplot at first level for ratio 4.95.....	65
Figure 5.23	3-D plot at second level for ratio 4.95.....	66
Figure 5.24	Counterplot at second level for ratio 4.95.....	66
Figure 5.25	3-D plot at third level for ratio 4.95.....	67
Figure 5.26	Counterplot at third level for ratio 4.95.....	67
Figure 5.27	3-D plot at fourth level for ratio 4.95.....	68

Figure 5.28	Counterplot at fourth level for ratio 4.95.....	68
Figure 5.29	3-D plot at final level for ratio 4.95.....	69
Figure 5.30	Counterplot at final level for ratio 4.95.....	69
Figure 5.31	Standard deviation change for ratio 1.97.....	70
Figure 5.32	Standard deviation change for ratio 2.95.....	71
Figure 5.33	Standard deviation change for ratio 4.95.....	71

TABLE LIST

Table 3.1	Type E Thermocouple.....	37
Table 3.2	Color coding according to IEC 304.....	38
Table 3.3	Tolerance classes according to IEC 60584.....	39
Table 4.1	Temperature Values.....	50

ABSTRACT

In this study, cross flow with a heated jet is analysed. The velocity ratio between heated jet and air flow is taken in different values. Air is used for both of the flows. Temperature values are measured by means of a thermocouple which is connected to a computer aided acquisition system.

After experimental study, temperature distribution at the cross section of the duct is plotted. For each ratio all temperature values are recorded and mixing process is observed. Additionally, the standard deviation is calculated for each ratio.

1. INTRODUCTION

One of the more basic processes in fluid mechanics is the mixing that occurs during the interaction of two intersecting stream of jets. The study of jets in cross flow is of big practical relevance to both engineering applications and natural phenomena. Plenty of examples can be found in aeronautics, industry and nature. Therefore, considerable attention has been given to the problems of jets issuing into cross flow. This is mainly because it is the basic configuration in many practical situations. Generally, the interest area is different for each different case. The main field of applications can be summarized as in the following list.

- i. V/STOL aircraft uses air jets for take-off lifting.
- ii. A hot stream of a gas in a pipe can be cooled easily by injecting jets of cool gas into flow.
- iii. Plume flows that are leaving chimney.
- iv. Turbine blade cooling.
- v. The roll-control of missiles.
- vi. A river which flows into ocean or sea.
- vii. Many biological systems.

This class of interaction processes, categorized as fluid or jet injection process, is usually associated with a nearby solid boundary surface. These injection processes are complicated by the fact that in their natural state they are almost invariably turbulent. [1]

This study is based on the heated jets in the cross flows which means very analogical to the cooling application. As it happens in the cooling case, the analysis focuses on mixing and interaction of two flows which have different temperatures and mix crossly. In this study a single jet is analysed by changing flow rate and temperature of it.

In fact, to understand the mixing phenomena better it should be studied the jet injected into a cross flow with an equal temperature. For this type of analyses experimental procedure is mainly based on the different velocity ratios. For each velocity ratio, different measurements are done and examined. In addition, the distribution of velocity, pressure and turbulence intensity should be investigated to show jet structure in detail. When this case has been studied it has been recognized that data revealed a complex structure. The structure was found to be strongly influenced by a pair of counter rotating eddies which were formed behind the jet. Thus the

rotational velocity field was also investigated in detail. However, in this study it will be analysed directly the heated jet and when it is necessary previous works that have been done about jet structure will be discussed.

As it is mentioned above in this study cross flow with heated jet in a combustion process will be analyzed. To do this, the jet was heated by means of a heater which was located just before the cross section. In this study, air has been chosen for both of the fluids. The flow rate of heated jet has been changed and for each case velocity ratios have been selected. To select velocity ratios previous experiments were considered and ratios have been directly taken from those. Air has been considered as ideal gas. Since air jet has been used instead of methane a correction factor has been considered and taken into account. Furthermore, because of the difference between ideal conditions and laboratory conditions a correction factor also has been taken into account for the air flow. After all corrections, the flow rates corresponding each velocity ratios have been calculated. A thermocouple has been placed in the duct and has been connected to acquisition devices of computer. By means of controller thermocouple has been moved inside the duct to get the different temperatures at different locations. The distributions of temperature at several sections have been measured by means of thermocouple and data have been analysed by means of computer.

2. LITERATURE REVIEW

2.1 General View

The study of jets in cross flow is of big practical relevance to both engineering applications and natural phenomena. Plenty of examples can be found in aeronautics, industry and nature. Therefore, considerable attention has been given to the problems of jets issuing into cross flow. This is mainly because it is the basic configuration in many practical situations. Main fields of application and their associated problems can be summarized in the following list.

- V/STOL aircraft use air jets to obtain lift for take off. During transition flight these jets are bent rearward, which changes the air flow around the aircraft body, causing a loss in lift and instability due to pitching moment. Choosing the number of jets and their locations are the most important problems in order to get maximum performance of the aircraft.
- A hot stream of a gas in a pipe or in a duct can be cooled simply and effectively by injecting jets of cool gas into it. In order to get a desired temperature distribution at a given section downstream of the jets, it is necessary to study the mixing of two flows.
- A plume leaving a chimney with substantial upward momentum is often by a cross wind (bent-over plume). In this air pollution problem it is important to calculate the ground level concentration for a given situation. It is customary to apply a suitable diffusion formula from a certain point at which the upward momentum of plume is negligible. The analysis of a jet in a cross flow can be applied to find the flow structure near this point as well as its location.
- A river with some contaminant materials, flowing into ocean or the lake with cross current, presents another problem of diffusion. In this case the main interest is in finding the polluted region and the degree of pollution (concentration distribution).

2.2 Previous Works

Numerous papers have been published about this subject. The problems have been analyzed can be classified into three groups. The first group concerns the determination of the jet centerline location either experimentally or analytically. The second group treats the problems relating to V/STOL aircraft. The third group investigates theoretically the rolling up of a jet due to a cross flow.

The complex interaction that takes place after a fluid is injected into a moving stream results in a three-dimensional flow field, even though the jet may be following a two-dimensional path. This, of course, complicates the job of experimentally measuring the complete flow field.

Gordier , Margason , and Platten and Keffer concentrated their efforts on measuring the trajectory of the jet for a wide range of injection angles and velocity ratios V_i/V_{∞} , the trajectory being one of the easiest jet properties to measure.[2] Jordinson, Keffer and Baines, Ramsey , Kamotani and Greber and Fricke, Wooler, and Ziegler measured Potential details of the interaction process and revealed the core very complex flow field that exists due to the pressures Injection and shear stresses in and around the jet flow.[3] [4] Very good descriptions of how the jet flow distorts and develops under the influence of the free-stream flow and body forces are given.

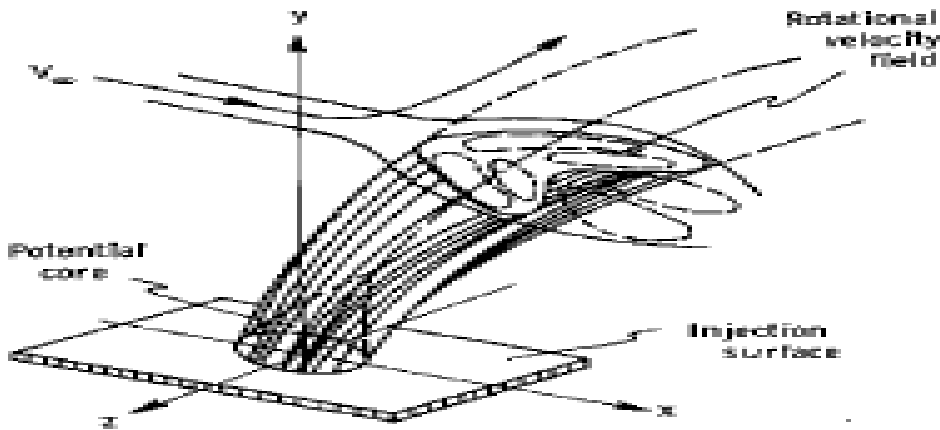


Figure 2.1 Diagram of the interaction resulting from jet injection into a cross flow.

The most detailed measurements of the flow field appear to be those of Keffer and Baines and Kamotani and Greber.[5] In particular, Kamotani and Greber examine the structure of the rotational velocity field which results because of the shearing action between the free-stream flow and the edge of the jet flow. The rotational velocity field, usually interpreted to be a pair of counterrotating vortices, is an interesting as well as important facet of the injection process; it affects the path of the jet as well as the mechanisms that govern entrainment. The data were reduced so that a measure of mass flux in the jet could be obtained, which in turn resulted in estimates of the rate that free-stream fluid is entrained into the jet structure. In addition to investigating the characteristics of the velocity field, Ramsey and Kamotani and Greber measured the temperature field resulting from the injection of a heated jet. [6]

It is important to note the limiting conditions of a jet injected at an arbitrary angle into a cross flow. If the angle between the jet axis and the direction of the free-stream velocity α goes to zero for a given value of V_i/V_c , the condition exists of a jet in a coflowing stream, that is, where the jet flow is parallel to the free stream. If the jet velocity becomes very large (V_i/V_∞) for a given α , the situation approaches that of a free jet. An indication of the magnitude of entrainment for a jet in a coflowing stream and for a free jet has been provided by Morton and Ricou and Spalding respectively.[7] [8]

In reviewing some of the theoretical methods available for modeling an injection process, it should be emphasized that a method is desired here which allows the injected fluid to be followed from its point of discharge to some point downstream where complete mixing takes place. At a minimum, from the method one should be able to estimate the three-dimensional (3-D) path of the injectant, to show how the jet size varies as it proceeds downstream, and to include basic heat-transfer mechanisms which allow the jet temperature to be predicted. The most advanced method would result in a complete and detailed description of the flow field resulting from an injection into a moving stream. This description could be accomplished by solving the full three-dimensional, turbulent, Navier-Stokes equations in an Eulerian framework, which requires the specification of the eddy viscosity field.

In order to avoid the complexities inherent with this approach, many studies have tried to theoretically model the gross features of the injection process by describing the fluid motion of the jet from the point of discharge in a Lagrangian framework. This procedure allows an estimate of jet properties to be obtained if the appropriate forces acting on the jet flow are accounted for. Since the jet path is the most obvious of the jet properties, it is natural that early attempts were concerned only with obtaining estimates of the trajectory. Abramovich, for example, obtained the trajectory of a jet which had a circular cross section at the injection point by balancing the centrifugal and blockage forces perpendicular to the trajectory. His basic argument was that the blockage effect of the jet flow on the free-stream flow could be approximated by assuming that the jet flow acts as a "solid" body inclined at some angle to the free stream. He accounted for the deformation of the jet cross section by assuming the shape to be elliptical and by specifying a growth rate for the cross-sectional area, which is necessary if only one force equation is used to obtain a solution for the trajectory. One of the serious drawbacks of this method is the assumption that the component of jet momentum perpendicular to the direction of the free-stream flow remains constant.

Two other forces acting perpendicular to the jet trajectory and which help govern the development of the jet flow are buoyancy force resulting from a difference in density between the jet and free-stream fluids and entrainment force resulting because of the free-stream fluid that is drawn into the jet structure. Theoretical trajectories were obtained by Reilly and Campbell and Schetz using procedures similar to those previously described but also accounting for the entrainment phenomenon; Campbell and Schetz, in addition, included the buoyancy force in their model.[9]

Since all these previous works utilized an assumed area growth based on experimental data obtained in the proximity of the injection point, they are not suitable for providing realistic trajectory information farther downstream. This deficiency can be avoided if, instead of assuming an area growth rate, a momentum conservation equation in the direction of the jet path is used; this equation is used in addition to the conservation equation in the direction perpendicular to the trajectory. Wooler, Burghart, and Gallagher, Hoult, Fay, and Forney, and Hoult and Weil used this procedure, solving force equations normal and parallel to the jet path

simultaneously to obtain a solution for the trajectory.[10] [11] [12] An added advantage of using these two force equations is that, if all the appropriate forces are accounted for, the solution procedure allows the jet flow properties to be estimated, as was done by Hirst and Campbell and Schetz .

In view of the preceding comments, the purpose of this way is to develop an integral method which accounts for natural fluid mechanisms such as turbulence, entrainment, buoyancy, and heat transfer in the conservation equations governing the jet flow. In particular, it is desirable to have a theory that utilizes the momentum conservation equation along the jet path.

2.3 Theoretical Development

The mathematical model allows the jet to penetrate into the cross flow and to bend over and spread under the influence of natural fluidic forces, and the jet velocity vector to approach the free-stream velocity vector at some point downstream from the jet exit. This capability is obtained by considering a section of jet fluid as a control volume similar to the approach used by Reilly.

The control volume is illustrated in figure 2.2 which depicts the trajectory of a jet injecting into a free-stream flow having a velocity V_0 taken Control to be spatially but not time dependent. The origin of the Cartesian (x,y,z) coordinate system is at the injection point, whereas the natural (s,n,t) coordinate system moves and rotates as it follows the path of the jet axis which is traced out by the jet velocity vector. The s -axis is located along the trajectory, the n -axis is oriented perpendicular to the trajectory in the direction of the radius of curvature of the trajectory, and the t -axis is perpendicular to both the s - and n -axes and completes the right-hand axis system. [13]

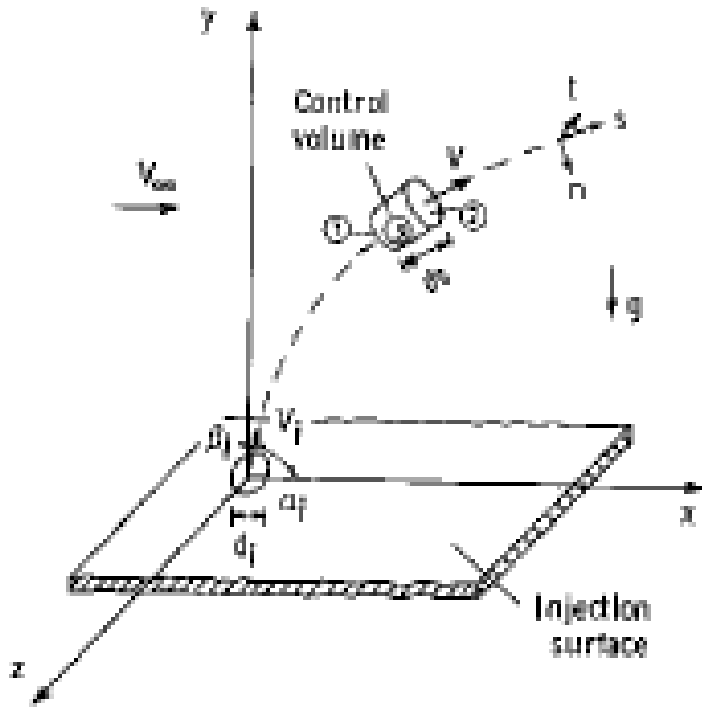


Figure 2.2 Cartesian and natural coordinate system

2.4 Different Kind of Trajectories

2.4.1 Two-Dimensional Trajectory

Experimental trajectory data obtained from different investigations of air jets are presented in figures below and show the two-dimensional paths of the turbulent jet for a range of injection velocities and orientations. These data were obtained from hot-wire measurements and, thus, represent the path that is traced by the maximum velocity in the jet flow. The measurements show that an increase in injection velocity or angle results in farther penetration of the jet into the free-stream flow. Theoretical trajectories were calculated with the same injection conditions as the experimental data and are in good agreement with the measured trajectories throughout the range of injection velocities and orientations.

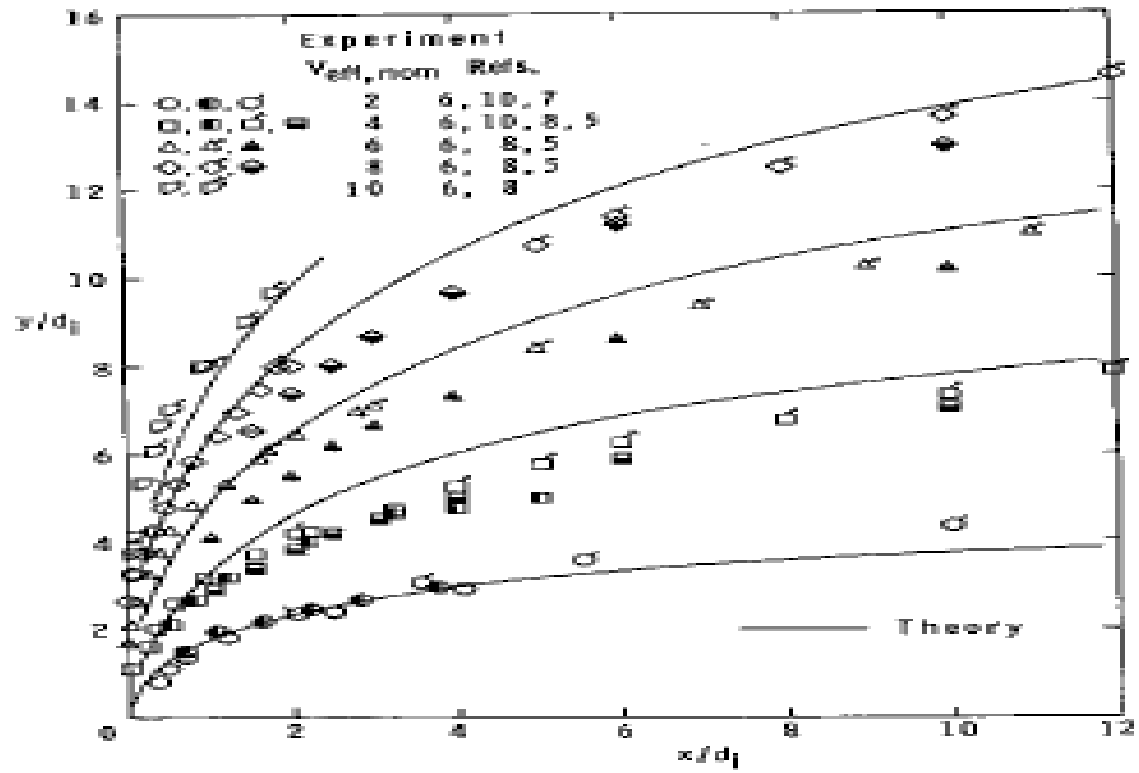


Figure 2.3 Experimental and Theoretical Trajectories of an Air Jet

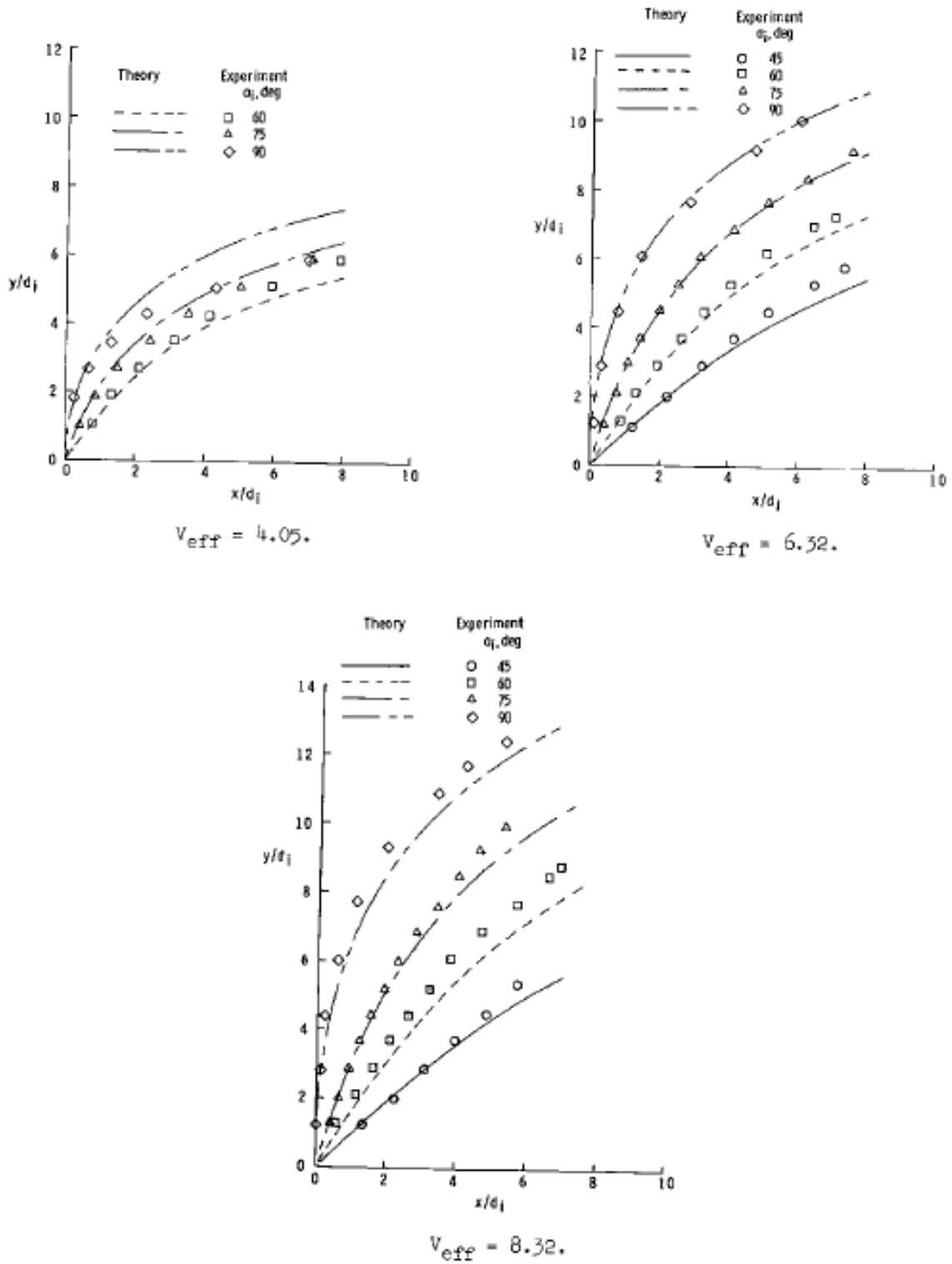


Figure 2.4 Experimental and Theoretical Trajectories of an Air Jet With Respect to Velocity Ratios

Theoretical trajectories calculated with the same injection conditions as the experimental data adequately represent the trend of increasing jet penetration with injection velocity and are in good agreement with the measured trajectories for the lateral and oblique injection processes.

2.4.2 Three-Dimensional Trajectory

Up until now all the theoretical trajectories that have been presented are, by definition, two dimensional; that is, they lie in a single plane. Figures below are presented to illustrate a three-dimensional path that results for a water injection process where a jet is injected normal to the mainstream and rotated 45° away from the vertical. An injection situation similar to this was observed in figure, where the theoretical trajectories are actually two dimensional because the Froude number of the jet flow is so large; or in other words, the buoyancy force is small compared to the momentum forces. In order to obtain a three-dimensional trajectory, particularly near the injection point, the Froude number of the jet flow must be small.

For the purpose of this demonstration, the heat transfer from the jet is ignored so that the jet density is assumed constant along the trajectory. Solutions for the governing conservation equations were obtained for $N_{Fr,i} = \infty$ and for $N_{Fr,i} = 10$; the projections of the resulting trajectories on the X-Y and X-Z planes are presented in figure below. For $N_{Fr,i} = \infty$, the projections on the two planes are equivalent which occurs only when $\beta_i = 45^\circ$ and the trajectory is two dimensional. Allowing ρ to be less than ρ_∞ leads to the second set of projections, which shows that decreasing the Froude number increases the penetration of the jet into the cross flow. The fact that the effect is more pronounced on the X-Y projection than on the X-Z projection is an indication that the triad of unit vectors associated with the natural coordinate system is tracing out a N_{Fr} three-dimensional path. In effect these unit vectors are "twisting" out of the plane where the two-dimensional trajectory obtained for $N_{Fr,i}$ is located. [14]

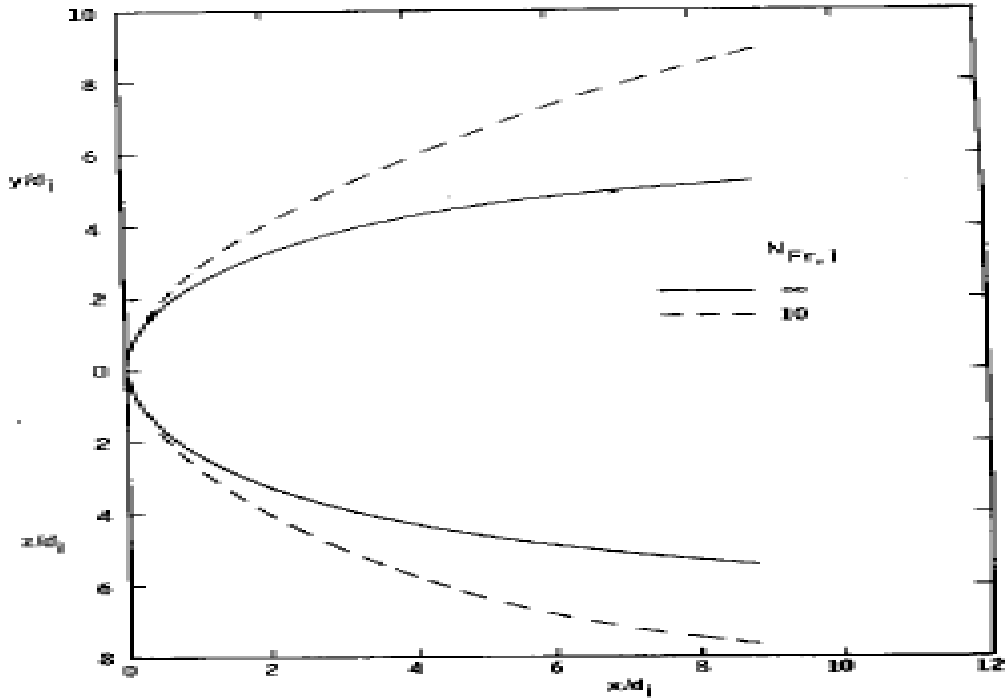


Figure 2.5 Effect of Froude Number on Jet Trajectory

Further evidence that these numerical results are consistent can be obtained by examining the dependent variables of the governing equations (u and w) and their gradients. This information is presented in figure below where the injection conditions are identical to those used in figure above, and the parameters in question are plotted as functions of distance along the trajectory. The solid curves represent the case where buoyancy force is zero ($N_{Fr,i} = \infty$) and are typical of the trends that result for injections with $0^\circ \leq \alpha_i \leq 90^\circ$ and $0^\circ \leq \beta_i \leq 90^\circ$. As noted, an increase in s/d_i results in a continual increase in u and a decrease in w , u and w approaching 1.0 and 0.0, respectively, for large s/d_i . These limits coincide with the jet velocity vector which becomes parallel to the free-stream velocity vector. In conjunction with these trends for u and w , du/ds and dw/ds are, respectively, positive and negative valued.

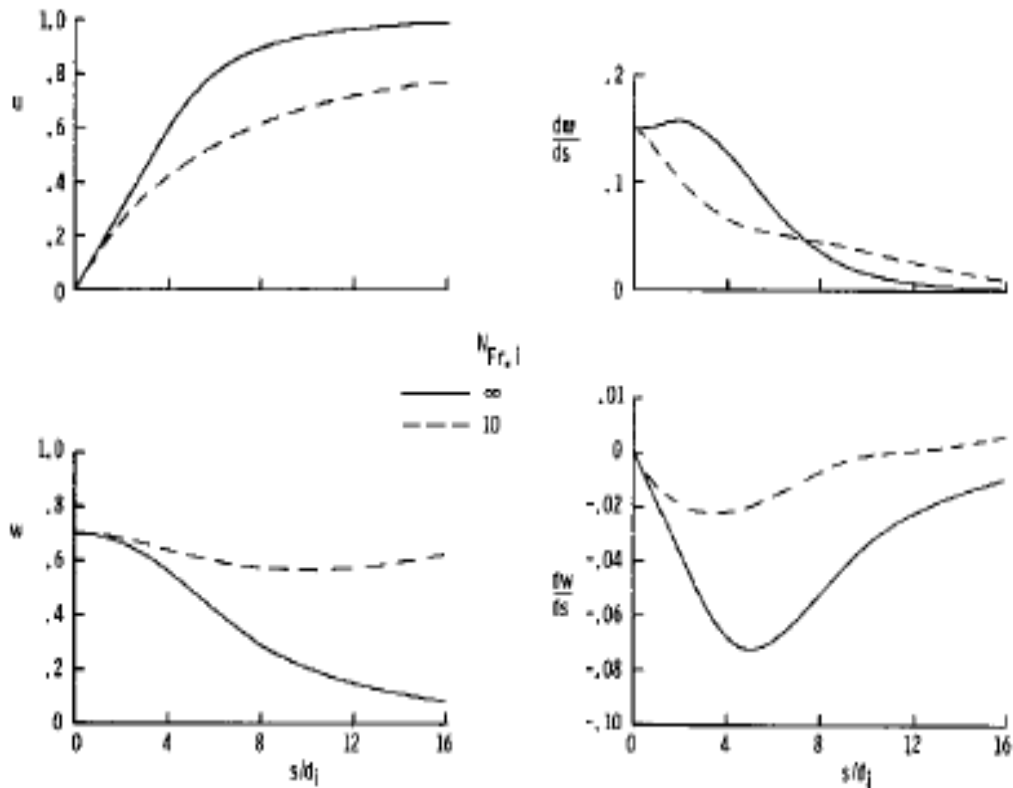


Figure 2.6 Effect of Froude Number on Variation of Jet Trajectory Parameters with distance along trajectory for $V_i/V_\infty = 4$, $\alpha_i = 90^\circ$ and $\beta_i = 45^\circ$

The dashed curves indicate what happens to the trajectory parameters when a sizable buoyancy force is considered. The fact that the values of u and w which result when $N_{Fr,i} = 10$ are, respectively, smaller and larger than the corresponding values when $N_{Fr,i} = \infty$ is indicative of the increase in penetration experienced by the jet when the buoyancy force is added. An interesting aspect of this situation is seen in the variation of w with s/d_i , where w reaches a minimum value at some point on the trajectory and then begins to increase. This is the same as saying that p achieves a maximum value and then begins to decrease. The trend of w with s/d_i is reflected in the dw/ds curve, where dw/ds changes from its usual negative sign to a positive value. This result is important because it signifies that buoyancy force is becoming dominant over the other forces acting on the jet flow. It is intuitively obvious that for the situation where buoyancy is the driving force, the jet path will tend toward the vertical so that w will be increasing with increase in s/d_i and dw/ds will be greater than zero. This can be shown explicitly

by letting $V_0 = u = du/ds = 0$ in the n-momentum equation and by solving the resulting expression for dw/ds . [15]

It is not possible to substantiate the trends discussed herein with results from other studies, since no experimental data exists for a jet with a three-dimensional trajectory. In the theoretical development, it was stated that the governing equations could apply to a jet following a three-dimensional path; however, no calculations of a three-dimensional trajectory were presented to support that claim.

2.5 Temperature Measurements

In fact, to understand the mixing phenomena better it should be studied the jet injected into a cross flow with an equal temperature. For this type of analyses experimental procedure is mainly based on the different velocity ratios. For each velocity ratio, different measurements are done and examined. In addition, the distribution of velocity, pressure and turbulence intensity should be investigated to show jet structure in detail. When this case has been studied it has been recognized that data revealed a complex structure. The structure was found to be strongly influenced by a pair of counter rotating eddies which were formed behind the jet. Thus the rotational velocity field was also investigated in detail. However, in this study it will be analysed directly the heated jet and when it is necessary previous works that have been done about jet structure will be discussed.

This study is based on the heated jets in the cross flows which means very analogical to the cooling application. As it happens in the cooling case, the analysis focuses on mixing and interaction of two flows which have different temperatures and mix crossly. In this study a single jet is analysed by changing flow rate and temperature of it.

3. TEMPERATURE MEASUREMENTS WITH THERMOCOUPLES

Monitoring temperature is a widespread and common engineering concept. Whether in a laboratory or factory, performing accurate, high-resolution, temperature measurements can be difficult and expensive. There are four most common temperature transducers: the thermocouple, the RTD (Resistance Temperature Detector), the thermistor and the IC (Integrated Circuit) sensor.

With the complexity of such systems it can become difficult to understand system accuracy, resolution, and rate of most temperature measurement solutions. Every temperature measurement application has different performance requirements and it is important to know exactly what errors exist in the system and how the resolution is being affected by noise. Even more useful is the ability to customize measurement settings to tune the system to the specific accuracy, resolution, and sampling rate needs. Thus, system performance can be divided into following categories: [16]

System Accuracy: It is important here to distinguish between system accuracy and measurement accuracy. While many products on the market will claim extremely high measurement accuracy, this is often simply the accuracy, or amount of error, in the actual measurement device. However, this specification often leaves out the error involved with other components of the system like the temperature sensor itself, the cold junction compensation (CJC) sensor, any cabling, SCXI hardware, or Switch hardware. It is important to know how to calculate the actual system accuracy, which is a combination of all these errors, so it is possible to determine the true tolerance on the final temperature reading.

System Resolution: This is the smallest detectable change in temperature that a system can detect. This is equivalent to $7\frac{1}{2}$ digits of resolution, but is dependent on a completely noiseless signal. Similar to system accuracy, the system resolution, or effective resolution, will depend on the level of noise and error in the signal due to the source, the cabling, and any other components in the system.

System Reading Rate: The system reading rate is the number of total temperature measurements that can be performed per second. This sampling rate therefore determines how quickly the system can show reaction to a change in temperature.

3.1 Comparison Of Temperature Measurement Sensors

As it has been mentioned above that four common types of sensor systems exist. The importance of the temperature sensors themselves in any thermal system is often overlooked. However, it is very important to understand the role of sensors in the system and what error they may introduce into the system. Therefore, it is important to have a look on different parameters of sensors. In the figure below, it is possible to see configurations of different types of sensors and their main characteristics. [17]

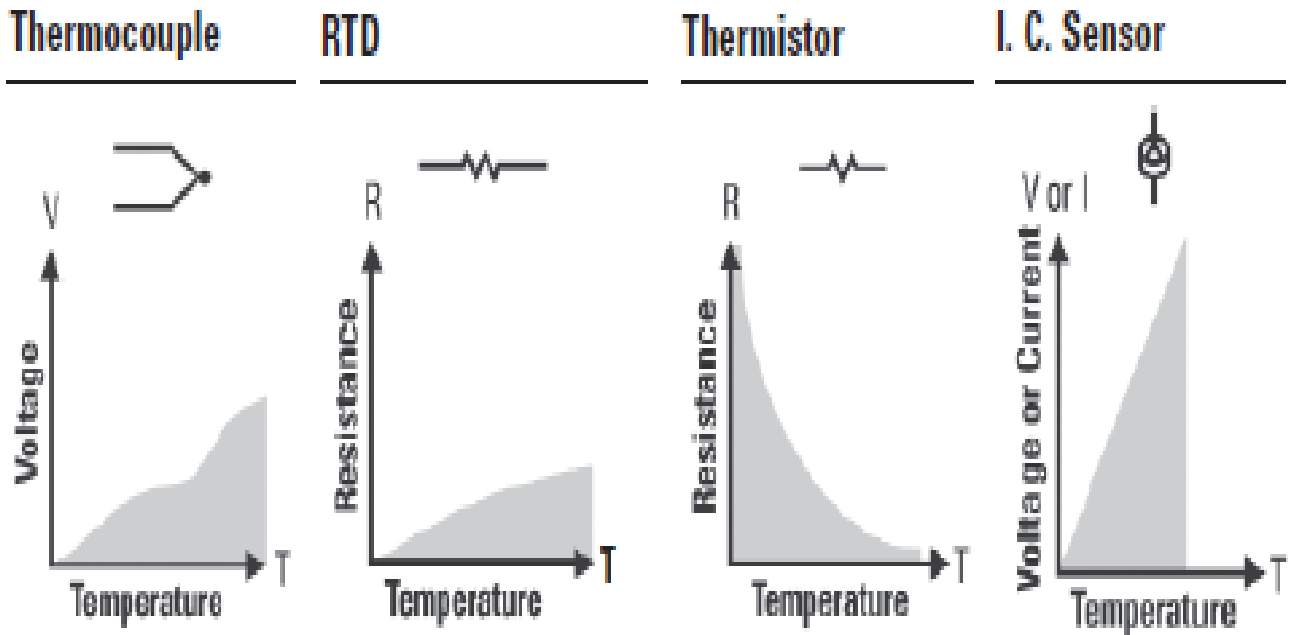


Figure 3.1 Temperature measurement sensors

3.2 Advantages and Disadvantages of Each Sensor

The main advantages of thermocouples are followings:

- Wide variety of physical forms
- Wide temperature range
- Self-powered
- Simple
- Rugged
- Inexpensive

The main disadvantages of thermocouples are followings:

- Non-linear
- Low voltage
- Reference required
- Least stable
- Least sensitive

The main advantages of RTD are followings:

- Most stable
- Most accurate
- More linear than thermocouple

The main disadvantages of RTD are followings:

- Expensive
- Slow

- Current source required
- Small resistance change
- Four-wire measurement

The main advantages of thermistor are followings:

- High output
- Fast
- Two-wire ohms measurement

The main disadvantages of thermistor are followings:

- Non-linear
- Limited temperature range
- Fragile
- Current source required
- Self-heating

The main advantages of I.C. sensor are followings:

- Most linear
- Highest output
- Inexpensive

The main disadvantages of I.C. sensor are followings:

- Power supply required

- Slow
- Self-heating
- Limited configurations [18]

3.3 Thermocouples

In a qualitative way, the temperature of an object is determined by the sensation of heat or cold felt by touching an object. Technically, temperature is a measure of the average kinetic energy of the particles in a sample of matter, expressed in units of degrees on a standardized scale. It is possible to measure temperature in many different ways that vary in cost of equipment and accuracy. One of the most frequently used temperature transducers is the thermocouple. Thermocouples are very rugged and inexpensive and can operate over a very wide temperature range. The fundamentals of thermocouples were established by Thomas Johann Seebeck in 1821 when he discovered that a conductor generates a voltage when it is subjected to a temperature gradient. Measuring this voltage requires the use of a second conductor material that generates a different voltage under the same temperature gradient. If the same material is used for the measurement, the voltage generated by the measuring conductor simply cancels that of the first conductor. The voltage difference generated by the two dissimilar materials can be measured and related to the corresponding temperature gradient. Based on Seebeck's principle, it is clear that thermocouples can only measure temperature differences and they need a known reference temperature to yield the absolute readings.

The Seebeck effect describes the voltage or electromotive force (EMF) induced by the temperature gradient along the wire. The change in material EMF with respect to a change in temperature is called the Seebeck coefficient or thermoelectric sensitivity. This coefficient is usually a nonlinear function of temperature.

The voltage is nonlinear with respect to temperature. However, for small changes in temperature, the voltage is approximately linear, or

$$\Delta V = S \Delta T$$

where ΔV is the change of voltage, S is the Seebeck coefficient, and ΔT is the change in temperature. S varies with changes in temperature, but, causing the output voltages of thermocouples to be nonlinear over their operating ranges. [19]

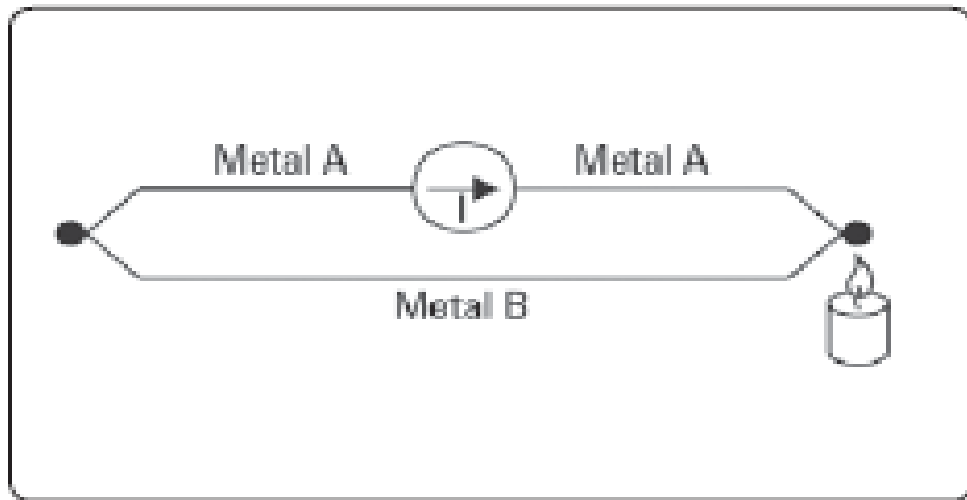


Figure 3.2 Seebeck Effect

3.3.1 Working Principles of Thermocouples

For measuring the temperature by using a thermocouple, it is not possible to connect simply the thermocouple to a voltmeter or other measurement system, because the voltage measured is proportional to the temperature difference between the primary junction and the junction where the voltage is being measured. Therefore, to know the absolute temperature at the thermocouple tip, the temperature where the thermocouple is connected to the measurement device has to also be known.

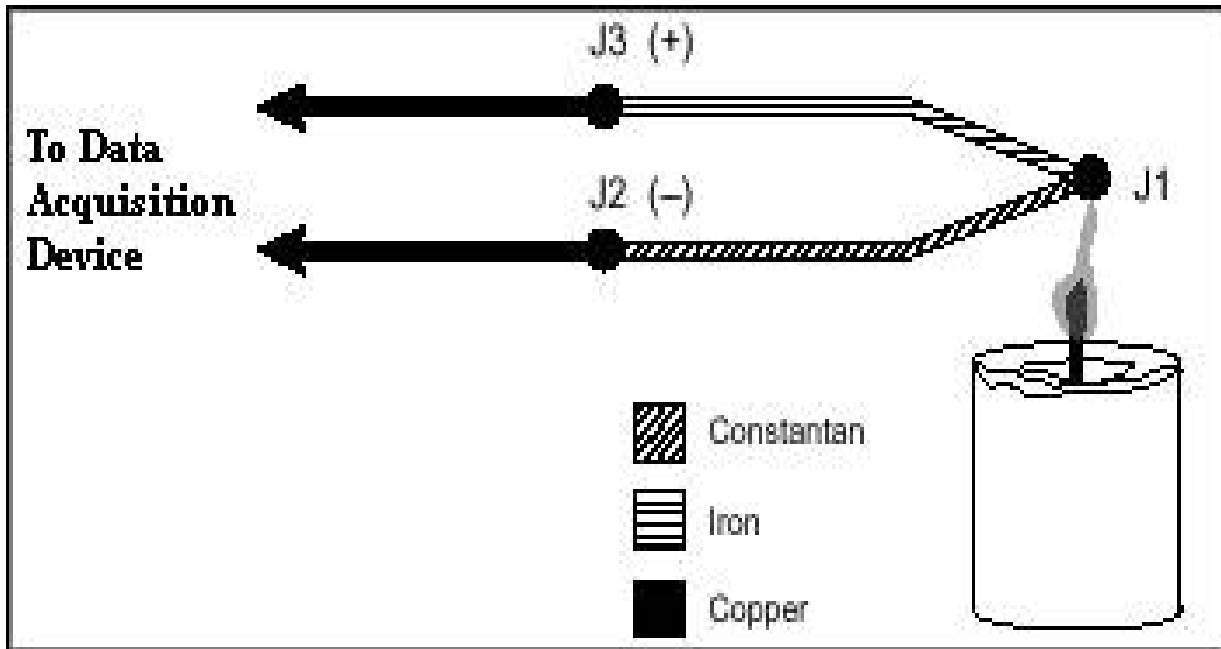


Figure 3.3 J- Type Thermocouple

Figure 3.3 illustrates a J-Type thermocouple in a candle flame that has a temperature to be measured. The two thermocouple wires are connected to the copper leads of a data acquisition device. In the circuit there are three dissimilar metal junctions: J1, J2, and J3. This leads to a Seebeck voltage between J3 and J2 which is proportional to the temperature difference between J1, which is sensing the temperature of the candle flame, and J2 and J3. J2 and J3 should be close enough each other so that they can be assumed to be at the same temperature. Because of the copper wire connection to both J2 and J3, there is no additional voltage contributed between the temperature difference of the J2/J3 junction and the point where the voltage is measured by the data acquisition device. To determine the temperature at J1, the temperatures of junctions J2 and J3 have to be known separately. Then, it is possible to use the measured voltage and the known temperature of the J2/J3 junction to infer the temperature at J1. [20]

3.4 Thermocouple Circuits

3.4.1 Cold-Junction Compensation (CJC)

Thermocouples require some form of temperature reference to compensate for these unwanted parasitic thermocouples. The term cold junction comes from the traditional practice of holding this reference junction at 0°C in an ice bath.

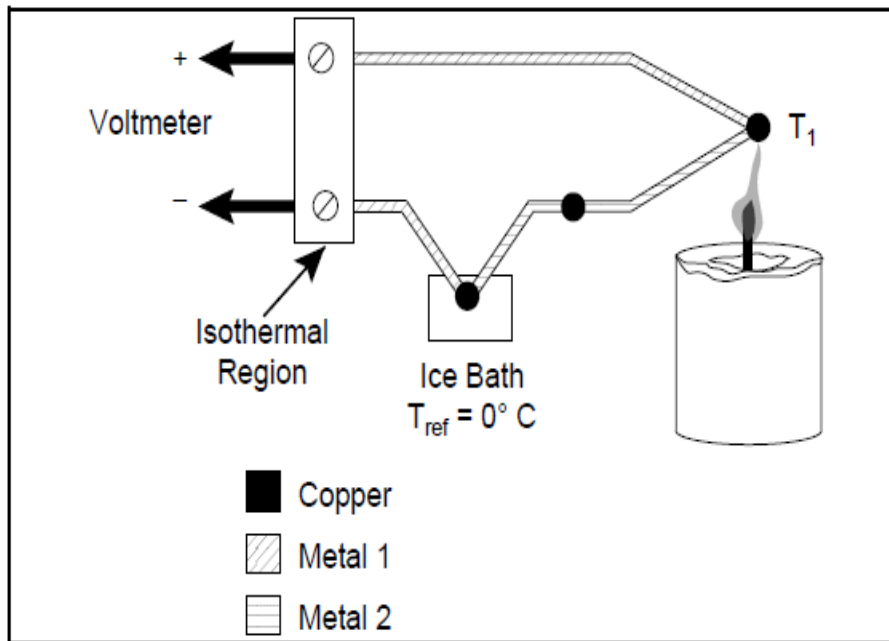


Figure 3.4 Traditional Temperature Measurement with Reference Junction Held at 0°C

In the figure 3.4, the measured voltage depends on the differences of temperatures T_1 and T_{ref} ; in the case CJC, T_{ref} is 0°C . It should be noticed that because the voltmeter lead connections are at the same temperature, or isothermal, the voltages generated at these two points are equal and opposite to each other. Thus, the net voltage error added by these connections is zero. Under these circumstances, if the measurement temperature is above 0°C , a thermocouple has a positive output; if it is below 0°C , the output is negative.

When the measurement the reference junction and junction have the same temperature, the net voltage is zero.

Although an ice bath reference is accurate, it is not always practical. There is a more practical way for measuring the temperature of the reference junction with a direct-reading temperature sensor and subtract the parasitic thermocouple thermoelectric voltage contributions. This process is called cold-junction compensation. It is possible to compute cold junction compensation simply by referring to advantage of some thermocouple characteristics. By using the Thermocouple Law of Intermediate Metals and making some simple assumptions, it is possible to see that the measured voltage depends only on the thermocouple type, the thermocouple voltage, and the cold-junction temperature. The measured voltage is obviously independent of the composition of the measurement leads and the cold junctions, J2 and J3. According to the Thermocouple Law of Intermediate Metals, illustrated in the figure below, inserting any type of wire into a thermocouple circuit does not affect on the output as long as both ends of that wire have the same temperature, or isothermal.

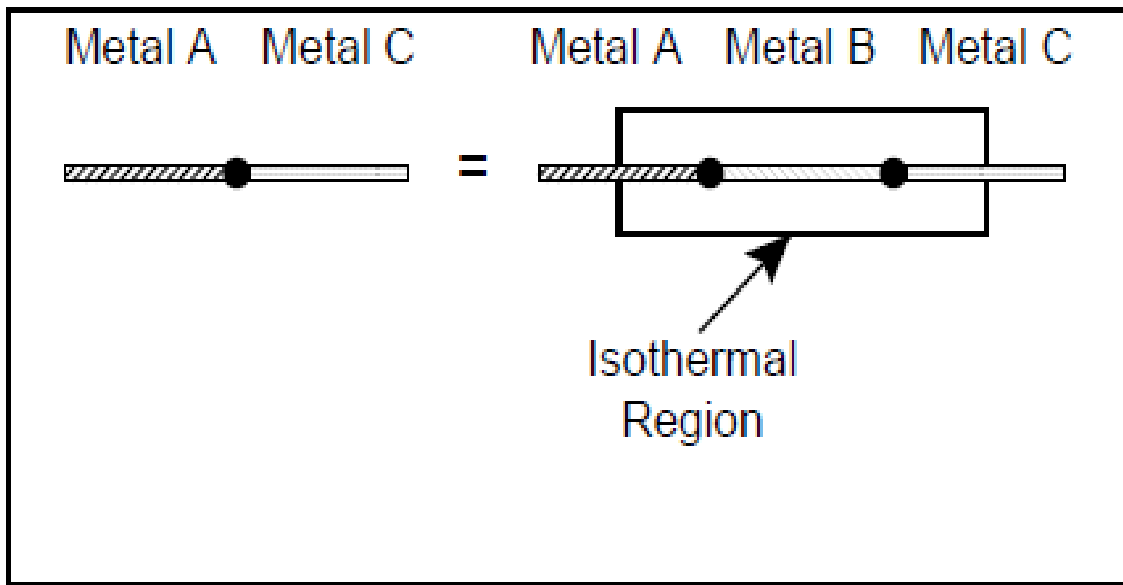


Figure 3.5 Thermocouple Law of Intermediate Metals

3.4.2 Software Compensation

In an alternative way, using software for cold-junction compensation is possible. After a direct-reading sensor measures the temperature of reference-junction, software can be used to add the appropriate voltage value to the measured voltage in order to cancel the parasitic thermocouple effects. Software compensation is the most versatile technique which exists for measuring thermocouples.

Thermocouples are mostly connected on the same block, copper leads are used throughout the scanner. Additionally, the technique is independent of the types of thermocouples chosen. In addition, when a data acquisition system is used with a built-in zone box, thermocouple is simply connected to a pair of test leads. All of the conversions are performed by the software instrument. The one disadvantage is that it requires a small amount of additional time to calculate the reference junction temperature. In the case maximum speed desired, hardware compensation can be used.

3.4.3 Hardware compensation

Rather than measuring the reference junction temperature and computing its equivalent voltage as done with software compensation, a battery is inserted to cancel the offset voltage of the reference junction. The combination of this hardware compensation voltage and the reference junction voltage is equal to that of a 0°C junction. The compensation voltage, e , is a function of the temperature sensing resistor, R_T . The voltage V is now referenced to 0°C, and may be read directly and converted to temperature by using the NIST tables. Another name used for this circuit is the electronic ice point. These circuits are commercially available for use with any voltmeter and with a wide variety of thermocouples. The major drawback is that a unique ice point reference circuit is usually needed for each individual thermocouple type. The figure below illustrates a practical ice point reference circuit that can be used in conjunction with a relay scanner to compensate an entire block of thermocouple inputs. All the thermocouples in the block must be the same type, but each block of inputs can accommodate a different thermocouple type by simply changing gain resistors.

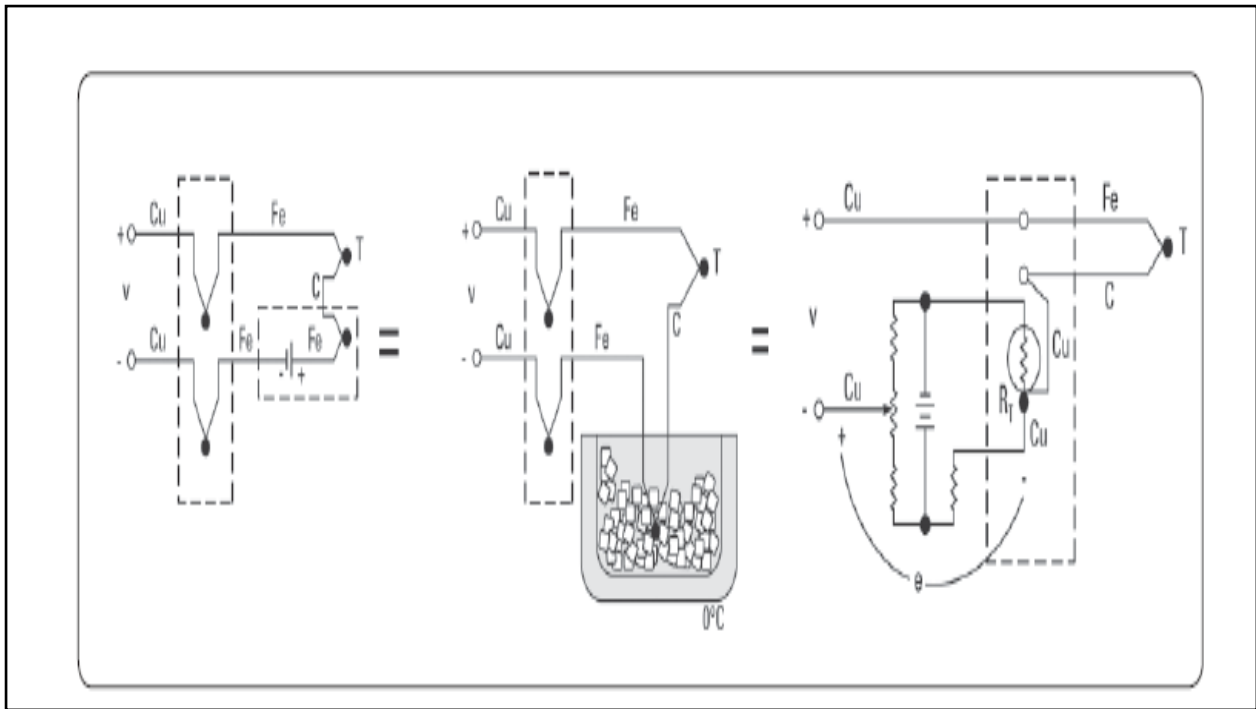


Figure 3.6 Hardware Compensation Circuit

The advantage of the hardware compensation circuit or electronic ice point reference is that the possibility of elimination of the need to compute the reference temperature. This cancels two computation steps and makes a hardware compensation temperature measurement somewhat faster than a software compensation measurement. However, advanced data acquisition and today's faster microprocessors designs continue to blur the line between the two methods, with software compensation speeds are challenging those of hardware compensation in practical applications.

3.4.4 Voltage To Temperature Conversion

Hardware and software compensation are used to synthesize an ice-point reference. Now, reading the digital voltmeter and converting the voltage reading to a temperature have to be done. Unfortunately, the temperature-versus-voltage relationship of a thermocouple is not linear. Output voltages for some popular thermocouples are plotted as a function of temperature in the figure 3.7 .

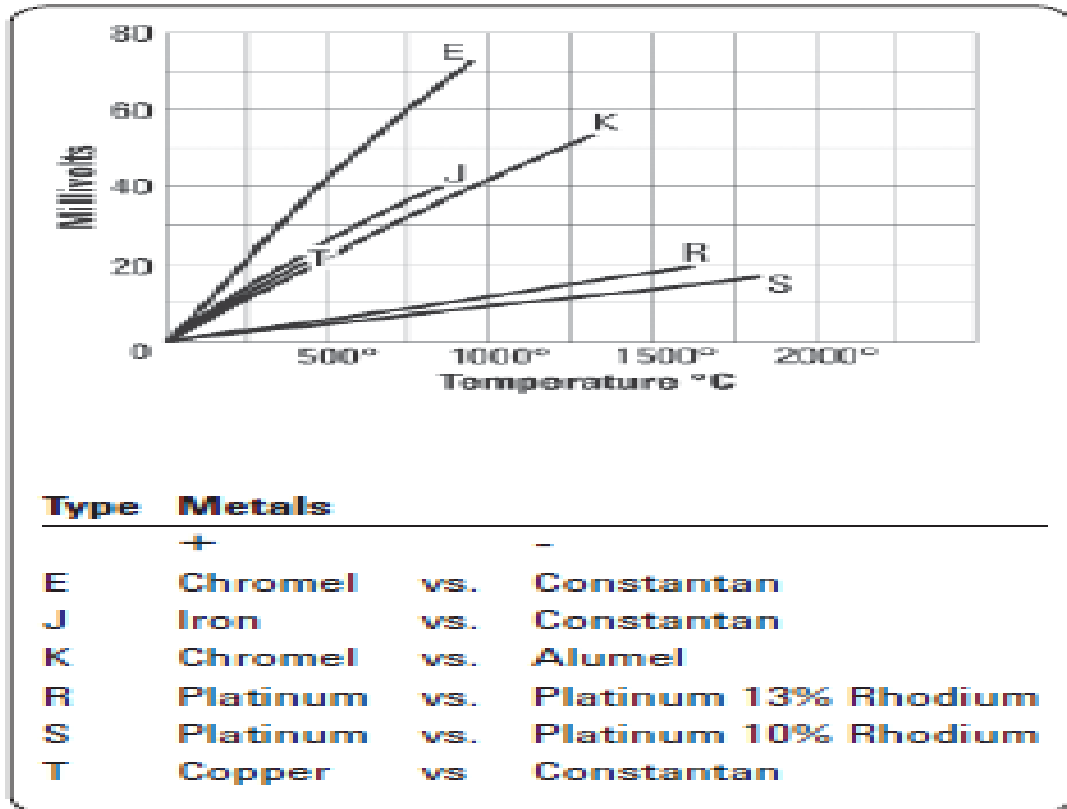


Figure 3.7 Thermocouple temperature vs. voltage graph

If the slope of the curve (the Seebeck coefficient) is plotted vs. temperature, as in the figure below, it becomes quite apparent that the thermocouple is a non-linear device. A horizontal line in figure below would indicate a constant α , in other words, a linear device.

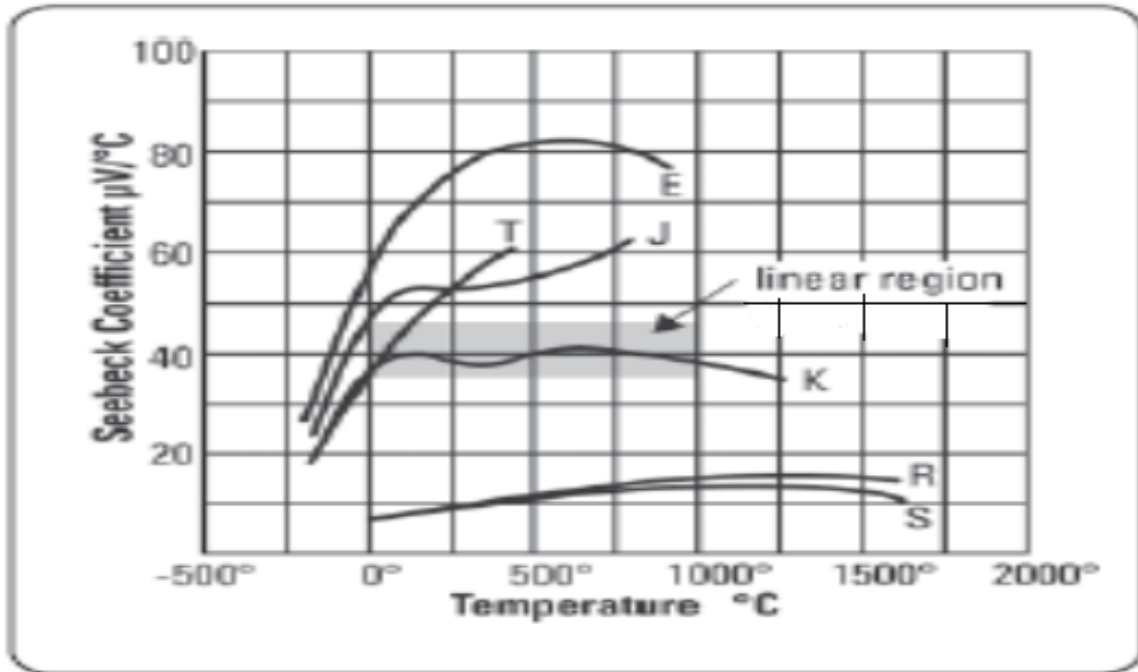


Figure 3.8 Seebeck coefficient vs. temperature

It is noticed that the slope of the type K thermocouple approaches a constant over a temperature range from 0°C to 1000°C . Consequently, the type K can be used with a multiplying voltmeter and an external ice point reference to obtain a moderately accurate direct readout of temperature. That is, the temperature display involves only a scale factor. By analysing the variations in Seebeck coefficient, it can be easily seen that using one constant scale factor would limit the temperature range of the system and restrict the system accuracy. Better conversion accuracy can be obtained by reading the voltmeter and consulting the NIST Thermocouple Tables. Each thermocouple type has its own table. As an example for these tables, for type E thermocouple NIST values can be seen in the table below.

Temperatures in °C (ITS-90)												
mV	.00	.01	.02	.03	.04	.05	.06	.07	.08	.09	.10	mV
0.00	0.00	0.17	0.34	0.51	0.68	0.85	1.02	1.19	1.36	1.53	1.70	0.00
0.10	1.70	1.87	2.04	2.21	2.38	2.55	2.72	2.89	3.06	3.23	3.40	0.10
0.20	3.40	3.57	3.74	3.91	4.08	4.25	4.42	4.59	4.76	4.92	5.09	0.20
0.30	5.09	5.26	5.43	5.60	5.77	5.94	6.11	6.28	6.45	6.61	6.78	0.30
0.40	6.78	6.95	7.12	7.29	7.46	7.63	7.79	7.96	8.13	8.30	8.47	0.40
0.50	8.47	8.64	8.80	8.97	9.14	9.31	9.48	9.64	9.81	9.98	10.15	0.50
0.60	10.15	10.32	10.48	10.65	10.82	10.99	11.15	11.32	11.49	11.66	11.82	0.60
0.70	11.82	11.99	12.16	12.33	12.49	12.66	12.83	12.99	13.16	13.33	13.50	0.70
0.80	13.50	13.66	13.83	14.00	14.16	14.33	14.50	14.66	14.83	15.00	15.16	0.80
0.90	15.16	15.33	15.50	15.66	15.83	16.00	16.16	16.33	16.49	16.66	16.83	0.90
1.00	16.83	16.99	17.16	17.32	17.49	17.66	17.82	17.99	18.15	18.32	18.49	1.00
1.10	18.49	18.65	18.82	18.98	19.15	19.31	19.48	19.64	19.81	19.98	20.14	1.10
1.20	20.14	20.31	20.47	20.64	20.80	20.97	21.13	21.30	21.46	21.63	21.79	1.20
1.30	21.79	21.96	22.12	22.29	22.45	22.61	22.78	22.94	23.11	23.27	23.44	1.30
1.40	23.44	23.60	23.77	23.93	24.10	24.26	24.42	24.59	24.75	24.92	25.08	1.40

Table 3.1 Type E Thermocouple

3.5 Types of Thermocouples

Wide variety of thermocouples is available which are differentiated according to type and construction. Each thermocouple has different characteristics and different application fields. Thus, it is important to select the most appropriate thermocouple type for the system that will be analysed. [21]

In the table below types of thermocouples, materials and color codes can be seen:



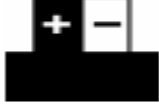




Thermal Pair – Types, Materials, Color Codes			
Element Type	Standard	Material Combination	Color Code
Type T	EN 60 584	Cu - CuNi	
Type E	EN 60 584	NiCr - CuNi	
Type J	EN 60 584	Fe - CuNi	
Type K	EN 60 584	NiCr - Ni	
Type S	EN 60 584	Pt10%Rh - Pt	
Type R	EN 60 584	Pt13%Rh - Pt	
Type B	EN 60 584	Pt30%Rh - Pt	

Table 3.2 Color coding according to IEC 304

Another classification parameter for thermocouples is the tolerance of them. According to IEC 60584, thermocouple types are subdivided into three tolerance classes:

Class	1
Tolerance (±) Type T	0.5°C or 0.004* t -40°C ... +350°C
Tolerance (±) Type E Type J Type K	1.5°C or 0.004* t -40°C ... +800°C -40°C ... +750°C -40°C ... +1000°C
Tolerance (±) Type R and S Type B	1°C or 1+(t-300)*0.003°C 0°C ... +1600°C
Class	2
Tolerance (±) Type T	1.0°C or 0.0075* t -40°C ... +350°C
Tolerance (±) Type E Type J Type K	2.5°C or 0.0075* t -40°C ... +900°C -40°C ... +750°C -40°C ... +1200°C
Tolerance (±) Type R and S Type B	1.5°C or 0.0025* t 0°C ... +1600°C +600°C ... +1700°C
Class	3
Tolerance (±) Type T	1.0°C or 0.015* t -200°C ... +40°C
Tolerance (±) Type E Type J Type K	2.5°C or 0.015* t -200°C ... +40°C -200°C ... +40°C
Tolerance (±) Type R and S Type B	4°C or 0.005* t +600°C ... +1700°C

Table 3.3 Tolerance classes according to IEC 60584

3.6 Error Estimation

Thermocouple output signals are typically in the millivolt range, and generally have a very low temperature to voltage sensitivity, which means that careful attention must be paid to the sources of errors which have severe impacts on the measurement accuracy. The primary sources of errors for the thermocouple measurement to take into account are noise, offset and gain errors, cold-junction compensation (CJC) accuracy, and thermocouple errors. [22]

3.6.1 CJC Errors

CJC errors represent the difference between the actual temperature at the point where the thermocouple is connected to the measurement device (the cold-junction temperature), and the measured temperature by the device. The CJC error is roughly a 1 to 1 contributor to the accuracy of the temperature measurement of the thermocouple, and is often one of the largest single contributors to the overall accuracy. The overall CJC error includes the error from the CJC temperature sensor (often a thermistor) used to sense the cold-junction temperature, the error from the device measuring the CJC sensor, and the temperature gradient between the cold-junction and the CJC sensor. Of these three errors, the temperature gradient between the cold-junction and the CJC sensor is generally the largest, and typically has the largest variation. The error from the CJC sensor can be a large contributor in many devices. The error from the temperature gradient between the cold-junction and the CJC sensor is where it generally has to be controlled mostly. A well-designed thermocouple device can often minimize this error considerably; however, the magnitude of this error still often depends on the environment in which the thermocouple device is used. Because the error comes from the temperature difference between the cold-junction and the CJC sensor, anything that can introduce a temperature gradient in a thermocouple device has affect on this error. Maintaining the thermocouple device in a stable environment with minimal temperature variation and low air flow is the best way to improve CJC accuracy. Adjacent heat sources, such as other instruments, can also impact the CJC accuracy.

Some devices have a single CJC sensor for many channels, while others may have multiple CJC sensors. As a general rule, devices with a low ratio of channels to CJC sensors are less susceptible to errors from temperature gradients. Device documentation can be referred for

specifics about the CJC accuracy and other recommendations for improving the overall CJC accuracy.

3.6.2 Offset and Gain Errors

Since output signals of thermocouples are often very close to 0 V and have a full input range that is measured in millivolts, offset errors from the measurement devices can largely contribute to overall accuracy. Many devices support a built-in autozero function that measures the internal offset of the circuit automatically. If a device supports built-in autozero, this is often the best way to compensate for offset errors and offset drift in the measurement device. The device documentation includes information about determining if autozero is supported. If autozero is not supported, careful attention should be paid to the contribution of offset error specification to the overall accuracy of the measurement device, and it should be ensured that the device is regularly calibrated.

Gain errors are proportional to the input voltage, so they generally have the largest impact when thermocouples are measuring temperatures at the edge of their supported range.

3.6.3 Noise Errors

Thermocouple output signals are typically in the millivolt range, that makes them susceptible to noise. Noise can be implemented either by the external environment or by the measurement device. Low-pass filters are commonly used in thermocouple data acquisition systems to effectively eliminate high-frequency noise in thermocouple measurements. For instance, low-pass filters are useful for removing the 50 and 60 Hz power line noise that is prevalent in many laboratory and manufacturing settings. For measurement devices with a large input range, it can also be improved the noise performance of the system by amplifying the low-level thermocouple voltages near the signal source (measurement point) to match the output range of the thermocouples. Since thermocouple output voltage levels are very low, a gain or input range for the device is selected to optimize the input limits of the analog-to-digital

converter (ADC). The output range of all thermocouple types is between -10 mV and 80 mV. Another source of noise is due to thermocouples being mounted or soldered directly to a conductive material such as steel, or submerged in conductive liquids such as water. When connected to a conductive material, thermocouples are particularly susceptible to common-mode noise and ground loops. Isolation helps prevent ground loops from occurring, and can dramatically improve the rejection of common-mode noise. With conductive materials that have a large common-mode voltage, isolation is required as non isolated amplifiers cannot measure signals with large common-mode voltages.

3.6.4 Thermocouple Errors

These errors come from the thermocouple. The voltage generated by the thermocouple is proportional to the temperature difference between the point where the temperature is measured and the point where it connects to the device. Temperature gradients across the thermocouple wire can introduce errors due to impurities in the metals, which can be large relative to most measurement devices. The thermocouple documentation should be referred to understand its accuracy impact to the overall measurement.

4. EXPERIMENTAL METHOD

4.1 Experimental Setup

The experiments were done within a transparent duct made by Plexiglas, with a cross-section of $40 \times 40 \text{ mm}^2$, which is aimed at simulating the intake duct of internal combustion engines while allowing full optical access. Compressed air was introduced into the duct from one side through a cylindrical pipe with inner diameter $d = 19 \text{ mm}$. A perforated grid (void ratio, area of the holes to the total area, equal to 60.5%) was inserted at the entrance of the duct, well upstream the jet injection to keep the turbulence approximately homogeneous and isotropic. In the reported experiments, the free stream velocity of the cross-flow U_{cf} was maintained constant at 1.66 ms^{-1} , with turbulence intensity $\approx 10\%$. The volume flow rate of inlet air in the duct was regulated and monitored with a rotameter, under controlled temperature ($\approx 20 \text{ }^\circ\text{C}$) and pressure (1 bar).

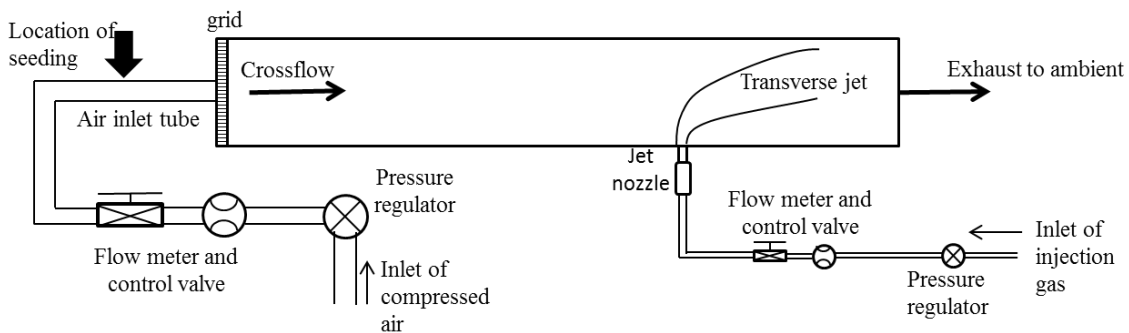


Figure 4.1 Schematic diagram of the duct and transverse jet injection system.

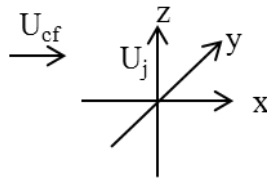


Figure 4.2 Coordinate system.

The gas jet entered the duct through a round pipe (inner diameter, $D = 6.4 \text{ mm}$; length, $L = 10 D$) whose outlet was mounted flush with the duct wall, oriented normally to it and with its

axis parallel to the Z direction in the coordinate system shown in Fig.1b, used throughout this report. The origin is located at the center of the jet pipe outlet. The jet axis was located in the mid plane, 330 mm downstream of the inlet section of the duct and 170 mm upstream of the exit. Jet exit velocity U_j (time averaged volume flux divided by the area of the jet) ranged from $\approx 2 \text{ ms}^{-1}$ to $\approx 10 \text{ ms}^{-1}$ in the present study.

The jet-to-cross-flow momentum flux ratio R is defined as: $R = \sqrt{\rho_j U_j^2 / \rho_{cf} U_{cf}^2}$

where the subscripts j and cf represent jet and cross-flow respectively, U_j is the time averaged volume flux divided by the area of the jet pipe outlet, and U_{cf} is the free-stream velocity of the cross-flow, defined through direct LDV measurements. The details of the investigated conditions are given also by the following Reynolds numbers:

- $Re_{cf} = \frac{U_{cf} l}{\nu_{air}}$ and l is the side length of the duct;
- $Re_j = \frac{U_j D}{\nu_{CO_2}}$ and D is the jet exit diameter;

4.2 Experimental Apparatus

As it is summarized above the duct, round pipe and thermocouple can be seen in the picture below. In this experiment from the round pipe heated jet will come and mix with the ambient air in the duct. The temperature of the mixed jet has been measured by using thermocouples. The heated jet has been provided by using a heater at the outlet of the round pipe just before the duct.

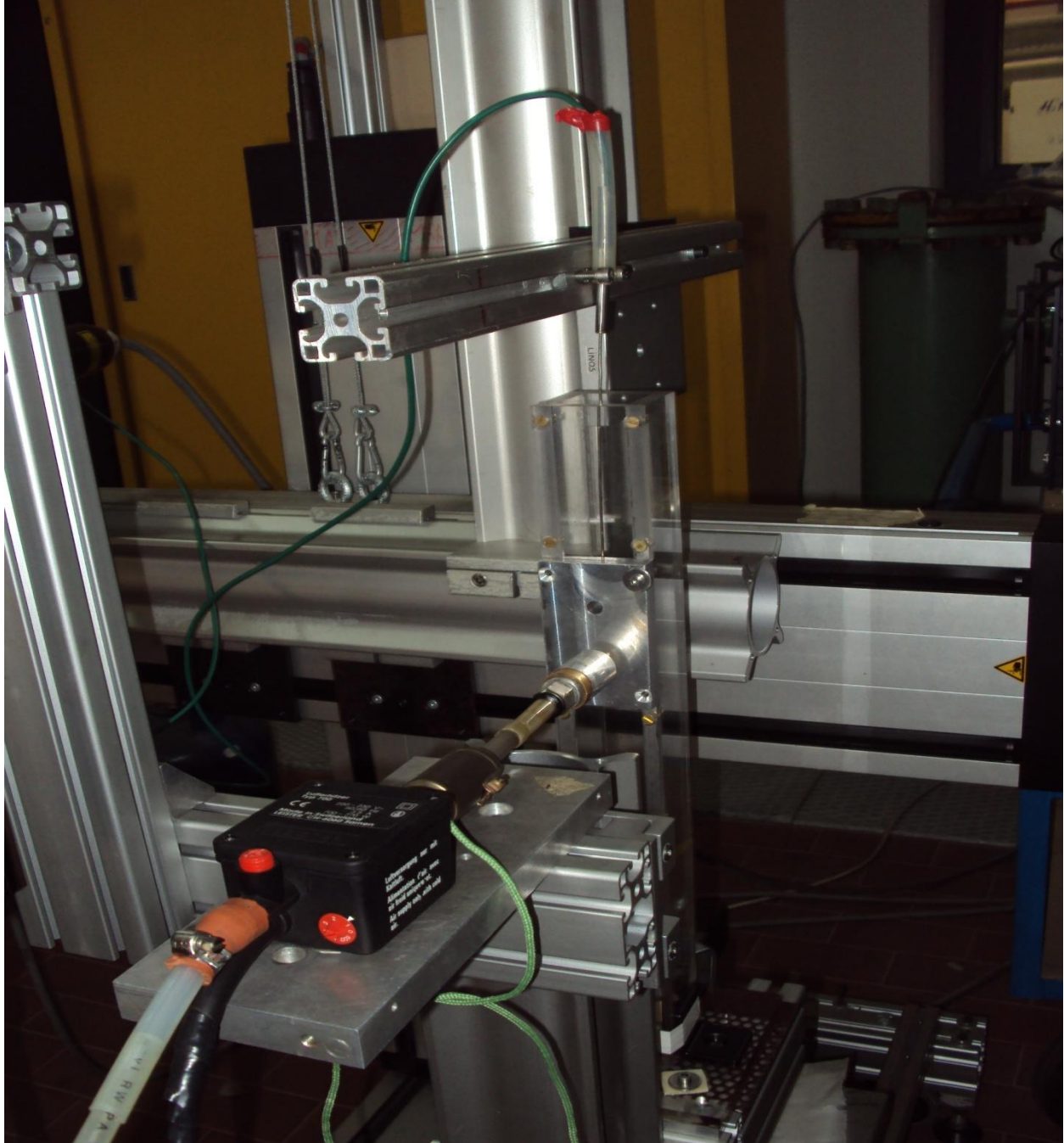


Figure 4.3 Air Mixing Apparatus

The flow rate of the heated jet and the ambient air has been adjusted with the valves. The pressure of both streams has been controlled regularly by using manometers inlet of the round pipe and duct. These valves and manometers can be seen in the figure 4.4.

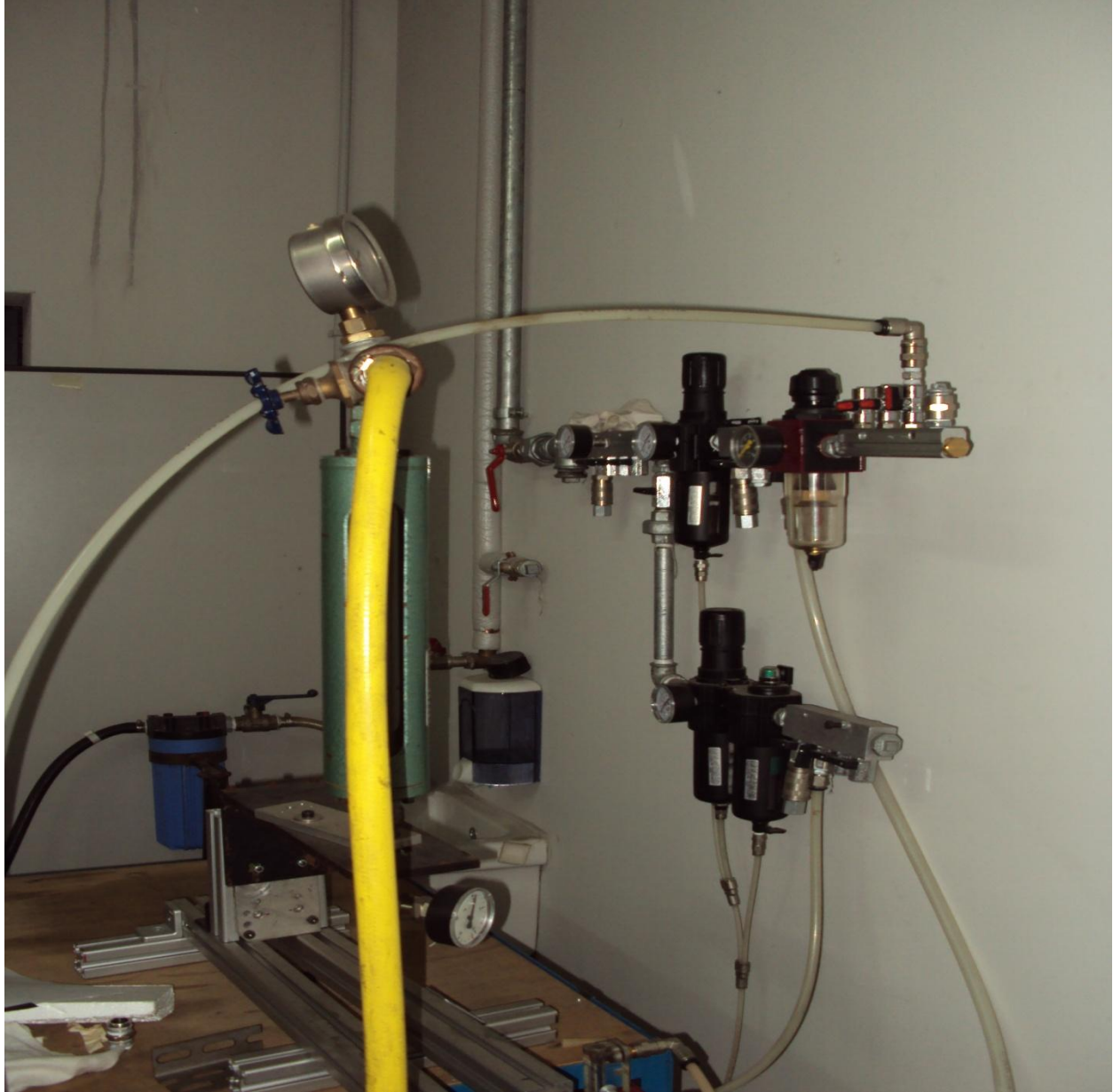


Figure 4.4 Control Valves and Manometers

After blowing heated jet and ambient air, the temperature of mixed jet has been measured by thermocouple. Thermocouple has been conducted to a computer acquisition system and all values have been recorded. The values have been taken by making a grid on the chosen section

of the duct. The thermocouple has been moved to every point in the grid by using a computer aided controller. The device and the computer used in the experiment are shown in the figure 4.5.



Figure 4.5 Controller of the Laser Doppler System and Computer

4.3 Experimental Procedure

Firstly, three velocity ratios were chosen by considering previous experiments done about this subject. These ratios are : 1.97, 2.95 and 4.95. For each ratio a correction was done due to pressure and density differences of heated jet and air. In this experiment, instead of methane, air was used as a fuel for simplicity. Thus different properties of air and methane have to be considered while doing experiment.

4.3.1 Correction Procedure

Air Reference Properties

$$\rho = 1.22 \text{ [kg/m}^3\text{]}$$

$$P = 1.01 \text{ [bar]}$$

$$T = 20 \text{ [}^\circ\text{C]}$$

Supplied Heated Jet Properties

$$\rho_{\text{jet}} = 1.03 \text{ [kg/m}^3\text{]}$$

$$T_{\text{jet}} = 150 \text{ [}^\circ\text{C]}$$

$$P_{\text{jet}} = 1.26 \text{ [bar]}$$

Supplied Air Flow Properties

$$\rho_{\text{air}} = 1.78 \text{ [kg/m}^3\text{]}$$

$$T_{\text{air}} = 19.5 \text{ [}^\circ\text{C]}$$

$$P_{\text{air}} = 1.5 \text{ [bar]}$$

Correction Coefficients for the air flow meters used in the experiments

$$\text{Pressure Coefficient} = (P_0/P_{\text{jet}})^{0.5} = 0.9$$

$$\text{Density Coefficient} = (\rho_0/\rho_{\text{jet}})^{0.5} = 0.8$$

Correction Coefficients for Supplied Air Flow

$$\text{Pressure Coefficient} = (P/P_{\text{air}})^{0.5} = 0.82$$

$$\text{Density Coefficient} = (\rho/\rho_{\text{air}})^{0.5} = 0.82$$

The maximum flow rate can be supplied in the system was read as $Q' = 4 \text{ [l/s]}$

The actual supplied flow rate $Q_a = Q' * 0.82 * 0.82 = 2.72 \text{ [l/s]}$

Duct Cross-Section Area: $A = 1600 \text{ [m}^2\text{]}$

Air flow velocity : $v_{\text{air}} = Q_a/A = 1.7 \text{ [m/s]}$

Jet velocity :

$$\text{For Ratio 1.97 : } v_{\text{jet}} = 1.97 * v_{\text{air}} * (\rho_{\text{air}}/\rho_{\text{jet}})^{0.5} = 4.4 \text{ [m/s]}$$

For Ratio 2.95 : $v_{jet} = 2.95 * v_{air} * (\rho_{air} / \rho_{jet})^{0.5} = 6.57$ [m/s]

For Ratio 4.95 : $v_{jet} = 4.95 * v_{air} * (\rho_{air} / \rho_{jet})^{0.5} = 11.03$ [m/s]

and actual jet flow rates are :

For Ratio 1.97 : $Q_{jet} = 8.47$ [l/s]

For Ratio 2.95 : $Q_{jet} = 12.7$ [l/s]

For Ratio 4.95 : $Q_{jet} = 21.3$ [l/s]

4.3.2 Thermocouple Positioning

After calculation of correction factors, the actual values of flow rates were determined and calculated as it is seen above. Then, the heated jet and air were supplied at corrected values and mixed in the duct. When air and jet mixed, temperature measurements were made by means of a thermocouple. These measurements were done at different sections in the duct. These sections are:

- Thermocouple was positioned at the same level with pipe center.
- Thermocouple was positioned at 6.4 mm (one pipe diameter) above the pipe center.
- Thermocouple was positioned at 12.8 mm (two pipe diameter) above the pipe center.
- Thermocouple was positioned at 32 mm (five pipe diameter) above the pipe center.
- Thermocouple was positioned at 64 mm (ten pipe diameter) above the pipe center.

Thermocouple was positioned by a controller which takes commands from a computer software. This controller allows thermocouple to move in three directions. At each section thermocouple made a grid which consists of 5 mm*5 mm squares. Thermocouple was colligated to a computer acquisition system. At each point of grid computer recorded temperature values. Even though acquisition system converts voltage values to temperature values (in Celsius) automatically, second calibration is needed.

4.3.3 Calibration of Thermocouple

As it is stated above a second calibration was done. The computer aided acquisition system takes values from thermocouple and converts them directly into temperature values. However, when these values were compared with the temperature values of the oil in the oven, a slight difference was seen between them. The oven has an oil reservoir. Oil is added into this reservoir and it is heated up to different high temperatures. Between every temperature enough time has to be passed for the stabilization of oil temperature degree. Then temperature values of oil were measured by means of computer acquisition system and mediums were taken. In addition, the temperature of oil was also measured with a thermocouple readout. A very small difference between oil temperature and values taken from thermocouple readout was observed. In the table 4.1, the values taken from computer, from thermocouple readout and oil temperature values can be seen.

Oil Temperature (°C)		Thermocouple Readout (°C)		Medium from PC (°C)	
30		29.8		33.19	
40		39.45		42.85	
50		49.3		52.48	
60		59.15		62	
70		69		71.42	
80		79.4		81.46	
90		89.3		91.26	

Table 4.1 Temperature Values

After taking these values manually and from computer a calibration curve was plotted.

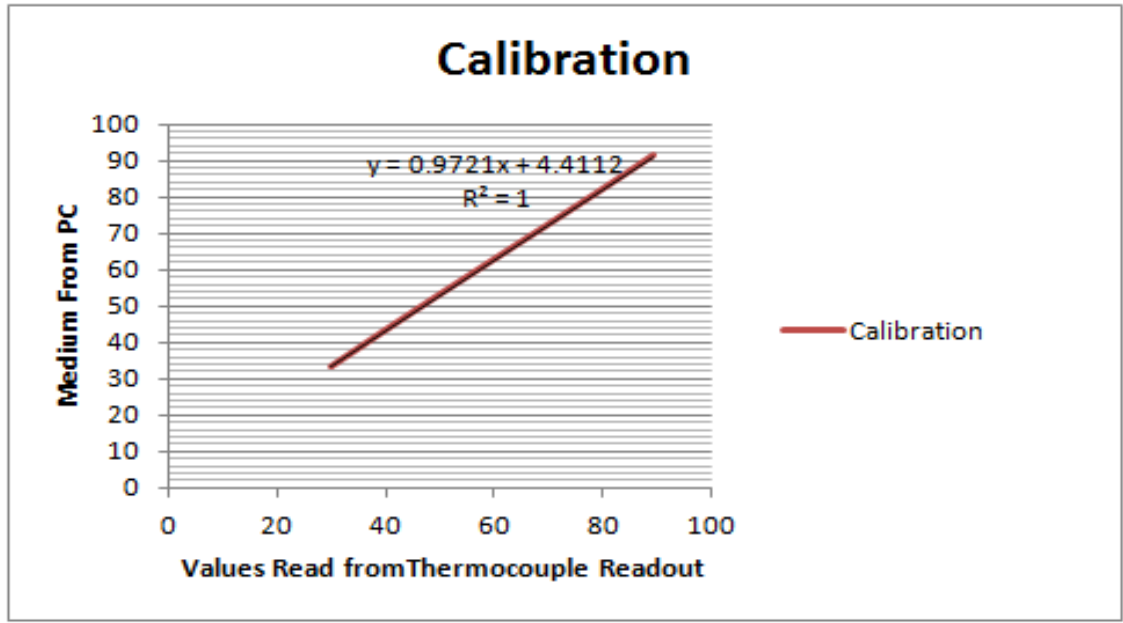


Figure 4.6 Calibration Curve

After calibration curve was plotted, all values recorded by computer were calibrated according to this curve. Then, all analysis was made according to calibrated values.

5. ANALYSIS AND RESULTS OF THE EXPERIMENTS

Once calibration curve was made, all temperature records were calibrated according to calibration curve. Temperature values were measured at each point of grid at all sections. Then, for each section and for each ratio 3-D and counterplots were made.

The measurement grid was made on the whole cross-section area of the duct. The grid consisted of 5*5 mm squares. The aim of the grid was to have all temperature values on the duct cross section. Additionally, grid shows temperature distribution of the mixed jet.

5.1 Analysis of Data for Ratio 1.97

As it is stated before temperature data was recorded at each section for each ratio. In the diagrams, 0 on the x axis shows where the nozzle placed. x and y axis shows the distance from the nozzle divided by pipe diameter. z axis shows the normalized temperature. At first three sections, grid was made with the dimensions 25*30 mm, at last two sections dimensions were 30*30 mm due to constraints of experimental apparatus (Duct size was: 40*40mm). For the same level with pipe center where thermocouple was positioned, contour plots and 3-D diagrams are followings. The temperatures have been normalized with the maximum temperature at the exit of the jet nozzle and the same normalization in all the following sections of the duct has been maintained.

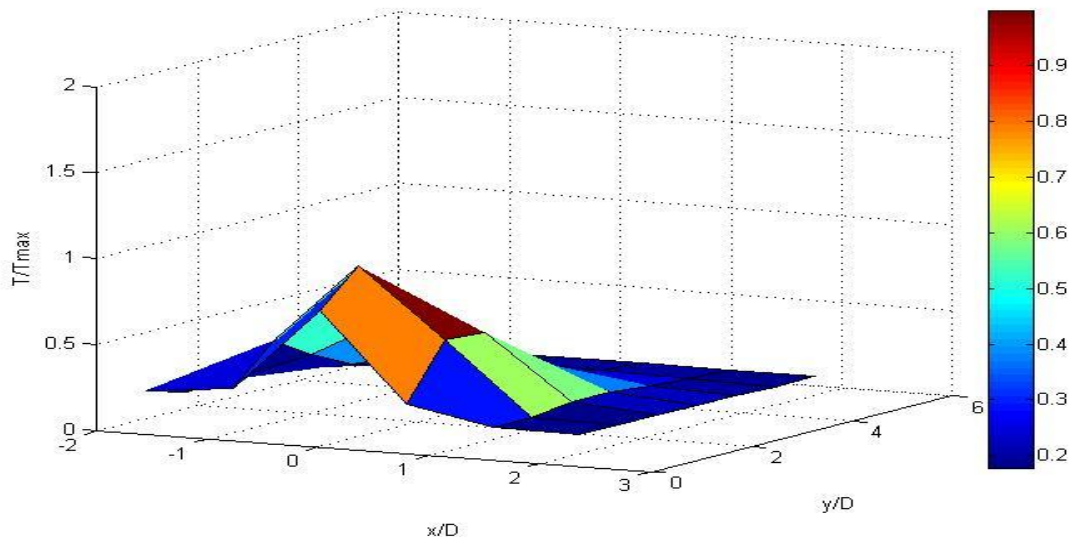


Figure 5.1 3-D plot at first level for ratio 1.97

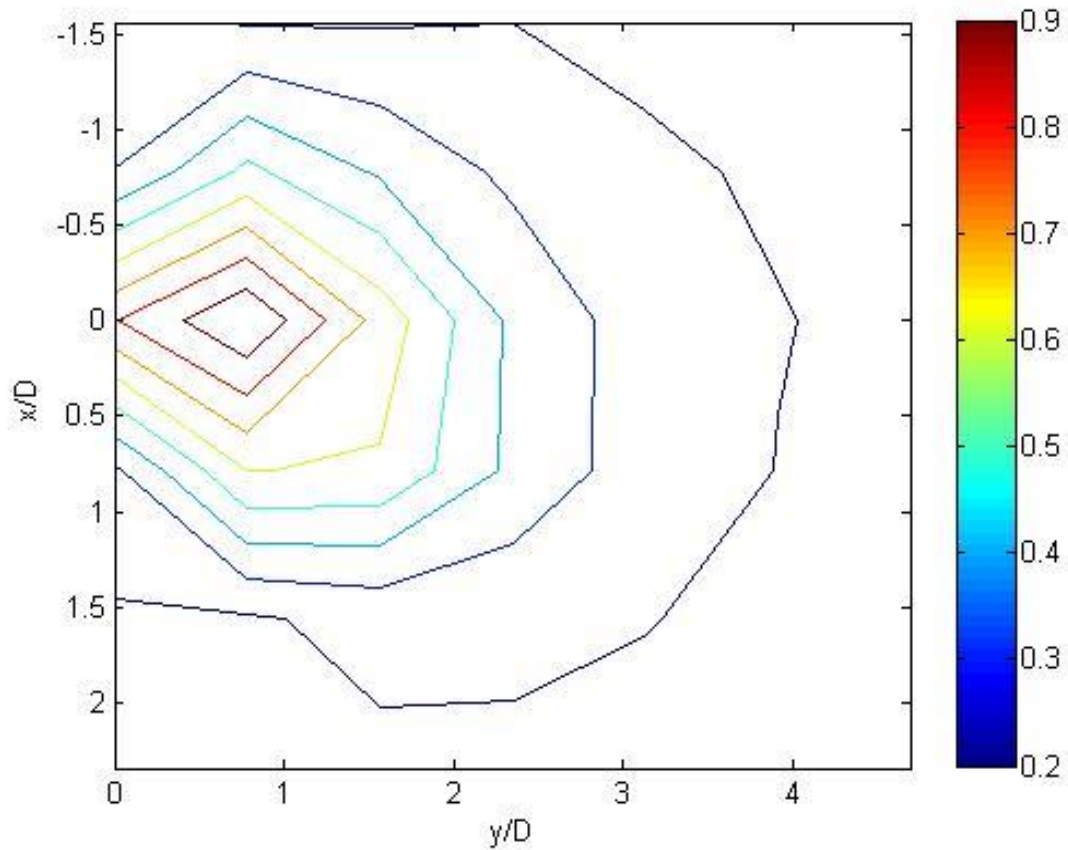


Figure 5.2 Contour plot at first level for ratio 1.97

As it is obviously seen in the figures above temperatures close to pipe exit are much higher than the temperatures close to duct walls. This shows that mixing process just began and temperature differences are considerably high.

In the following figures thermocouple was positioned at 6.4 mm (one pipe diameter) above the pipe center.

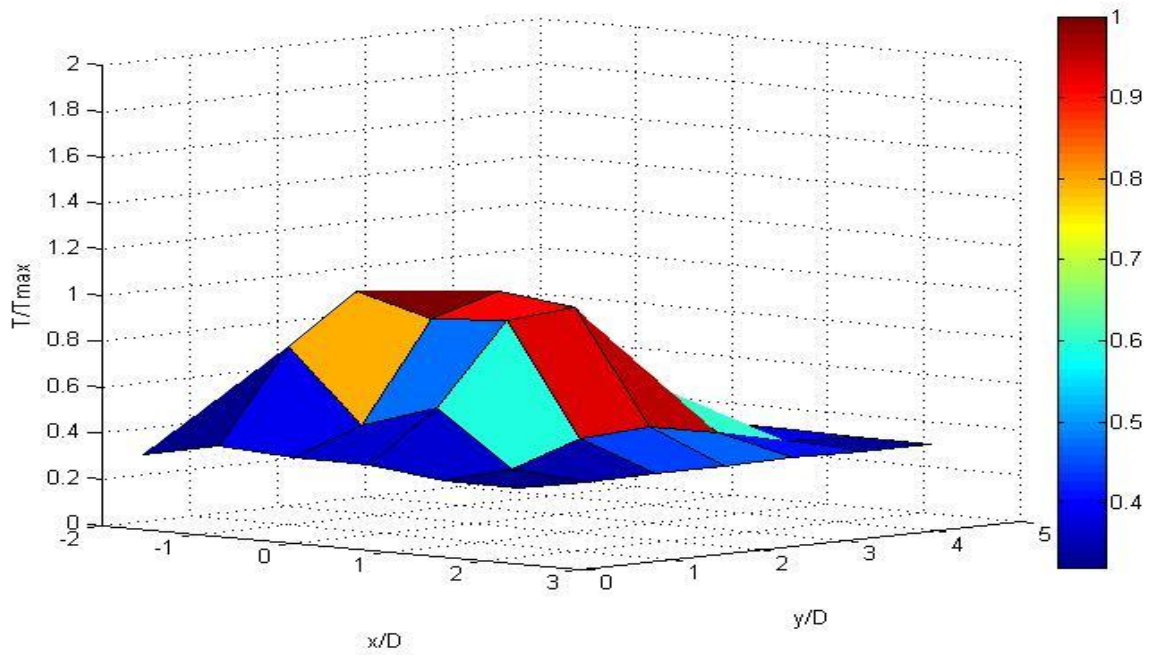


Figure 5.3 3-D plot at second level for ratio 1.97

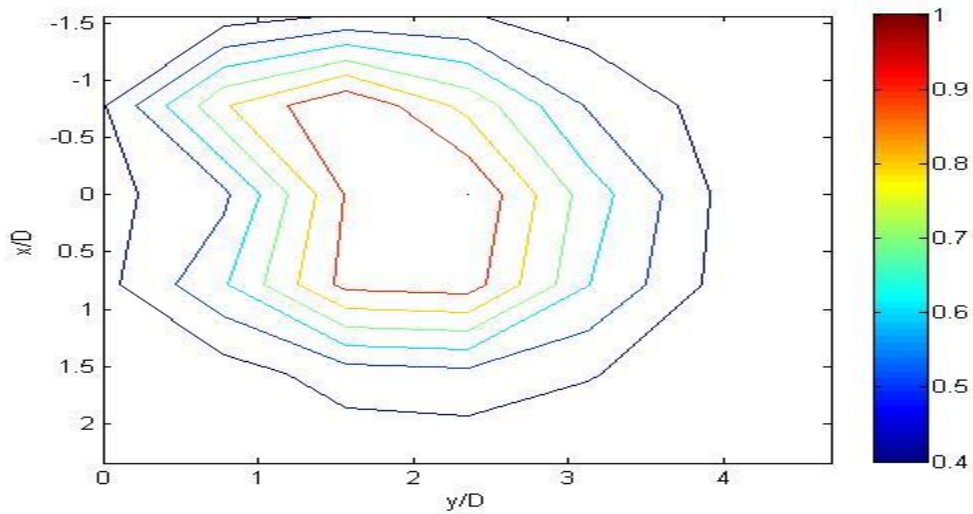


Figure 5.4 Contour plot at second level for ratio 1.97

As it can be seen in the figures above temperature differences are still high. However, if it is compared with the first level, there is slight decrease in temperature differences.

In the following figures thermocouple was positioned at 12.8 mm (two pipe diameter) above the pipe center.

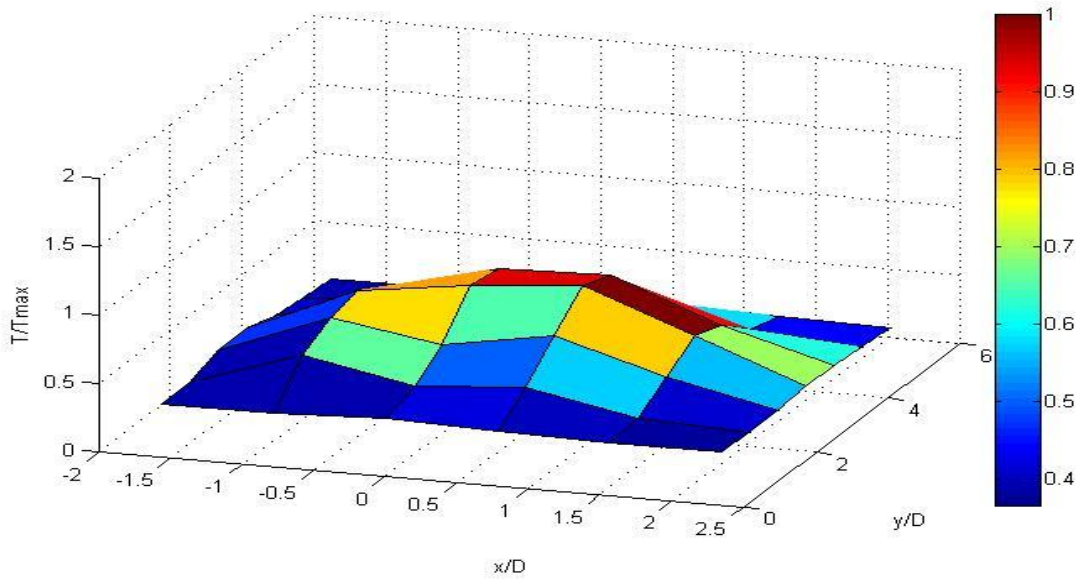


Figure 5.5 3-D plot at third level for ratio 1.97

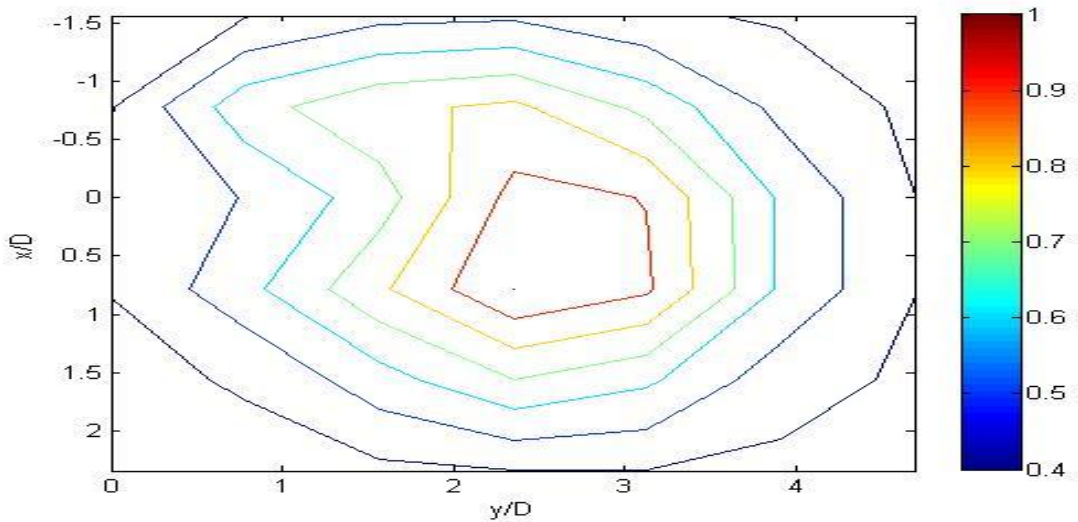


Figure 5.6 Contour plot at third level for ratio 1.97

As it can be seen in the figures above temperature differences decrease more. At this level development of mixing is observed better. It is observed that maximum temperature

moved to the center of the duct due to heat exchange in the vicinity of the wall and due to the motion of the jet.

In the following figures thermocouple was positioned at 32 mm (five pipe diameter) above the pipe center.

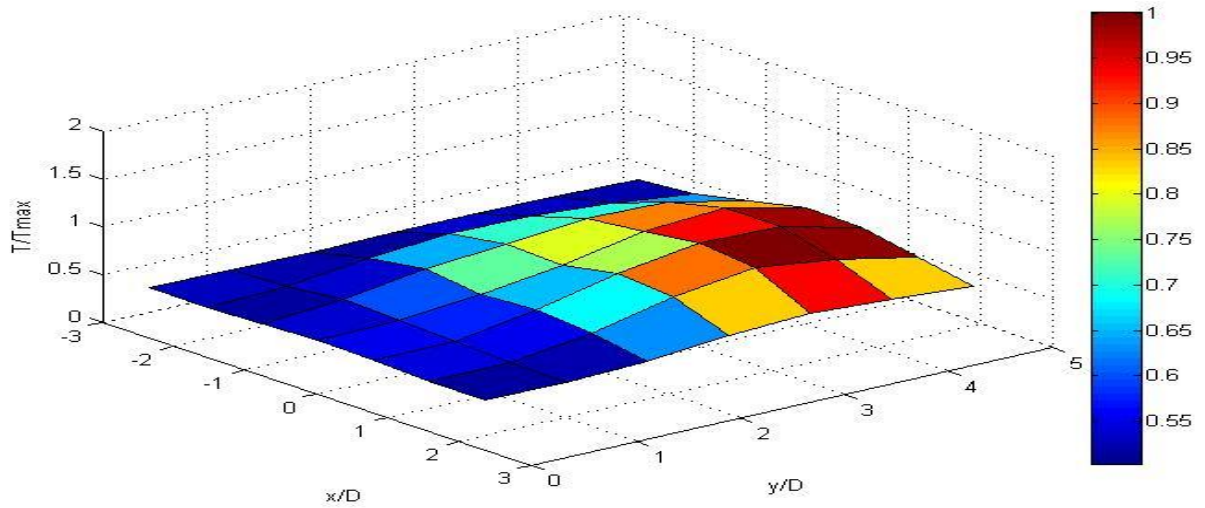


Figure 5.7 3-D plot at fourth level for ratio 1.97

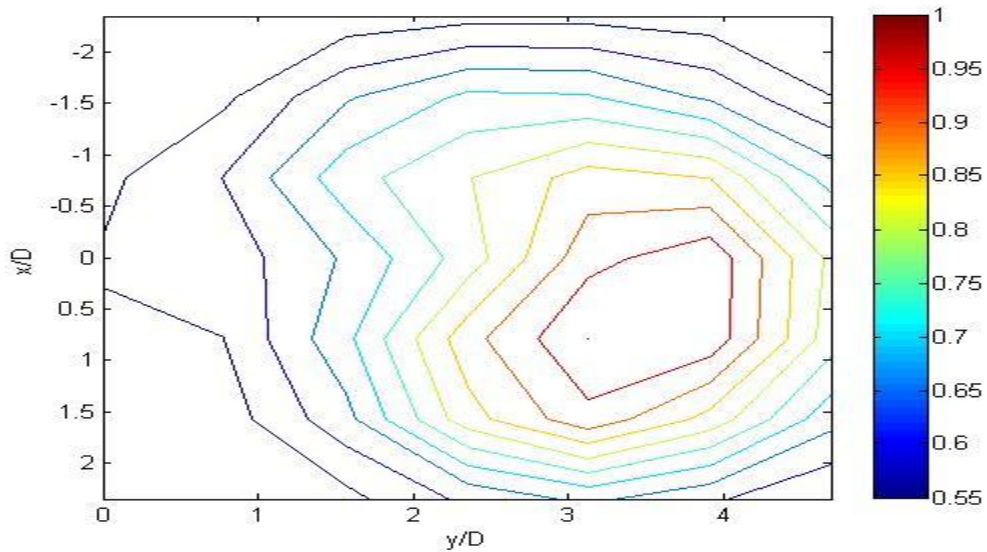


Figure 5.8 Contour plot at fourth level for ratio 1.97

As it can be seen in the figures above, mixing process almost completed. There are still temperature differences but when compared with lower levels they are smaller. At this level the highest temperature are close to wall that is opposite to the pipe exit.

In the following figures thermocouple was positioned at 64 mm (ten pipe diameter) above the pipe center.

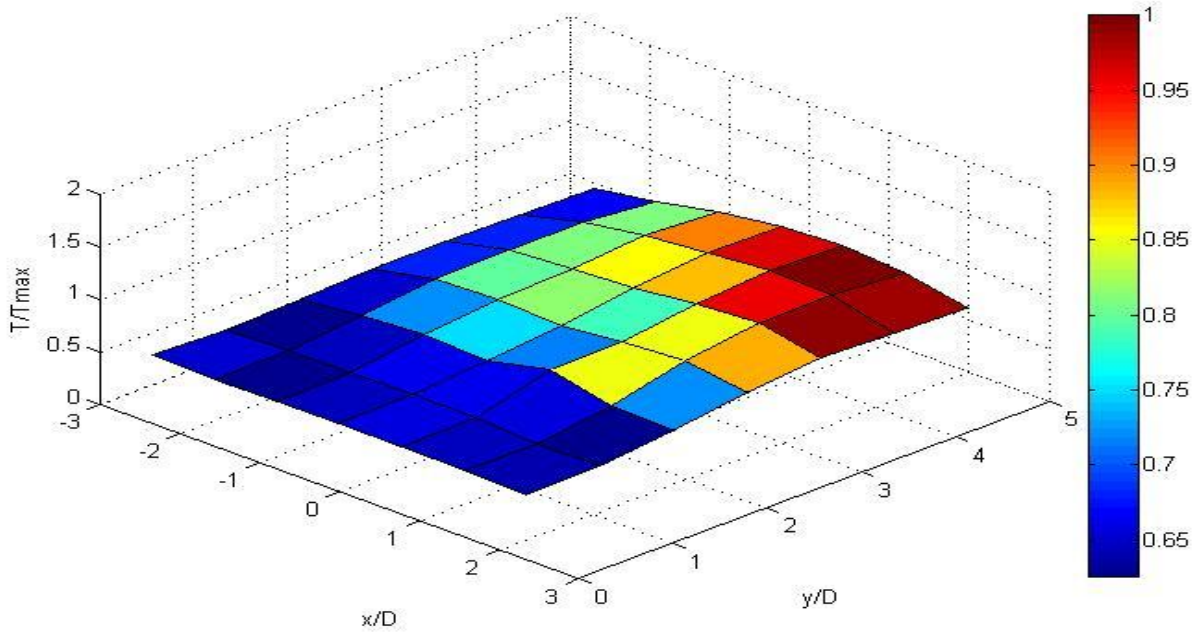


Figure 5.9 3-D plot at final level for ratio 1.97

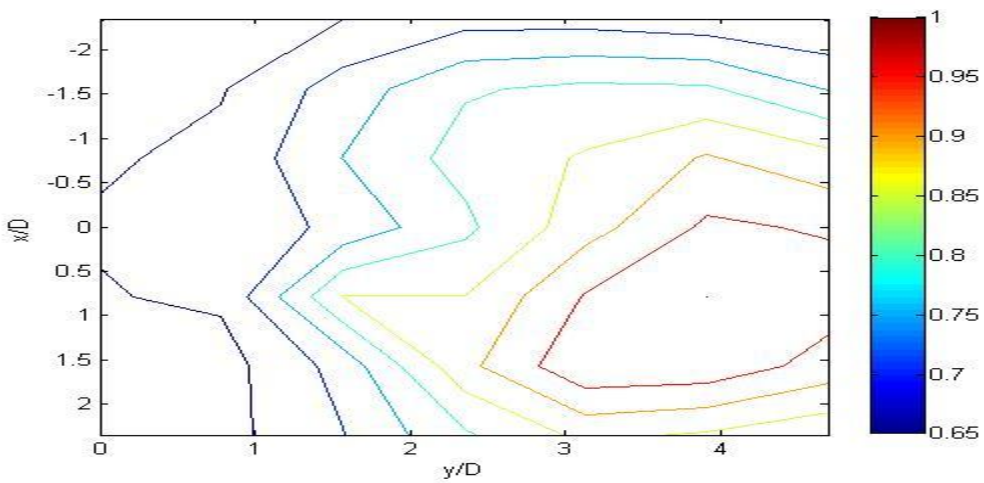


Figure 5.10 Contour plot at final level for ratio 1.97

As it can be obviously seen at this section temperature differences are the lowest. Mixing process can be considered as complete. The change between fourth level and final level is respectively small. The highest temperature values are close to wall that is opposite to the pipe exit. The heat transfer between heated jet and air is almost finished. Thus, this section can be considered as exit section of the duct.

5.2 Analysis of Data for Ratio 2.95

The same experiment was done with different ratios to observe mixing better. After the first experiments done, another experiment with ratio 2.95 was done by following the same procedure.

In the following figures thermocouple was positioned at the same level with pipe center.

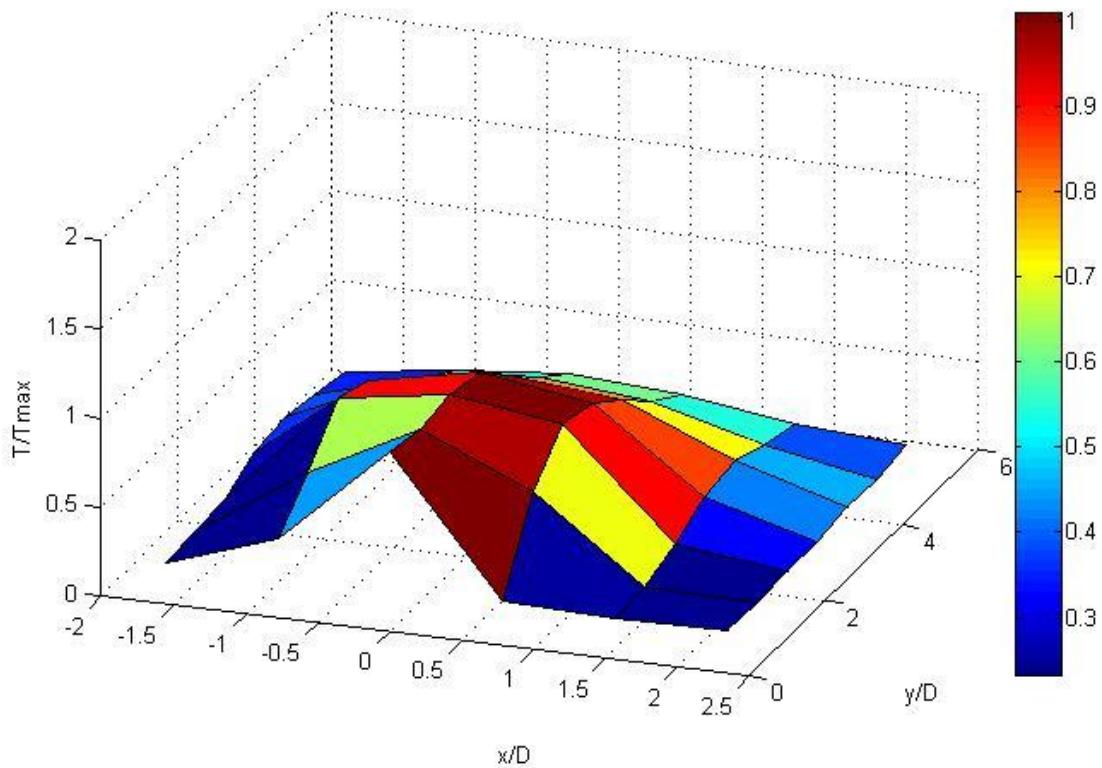


Figure 5.11 3-D plot at first level for ratio 2.95

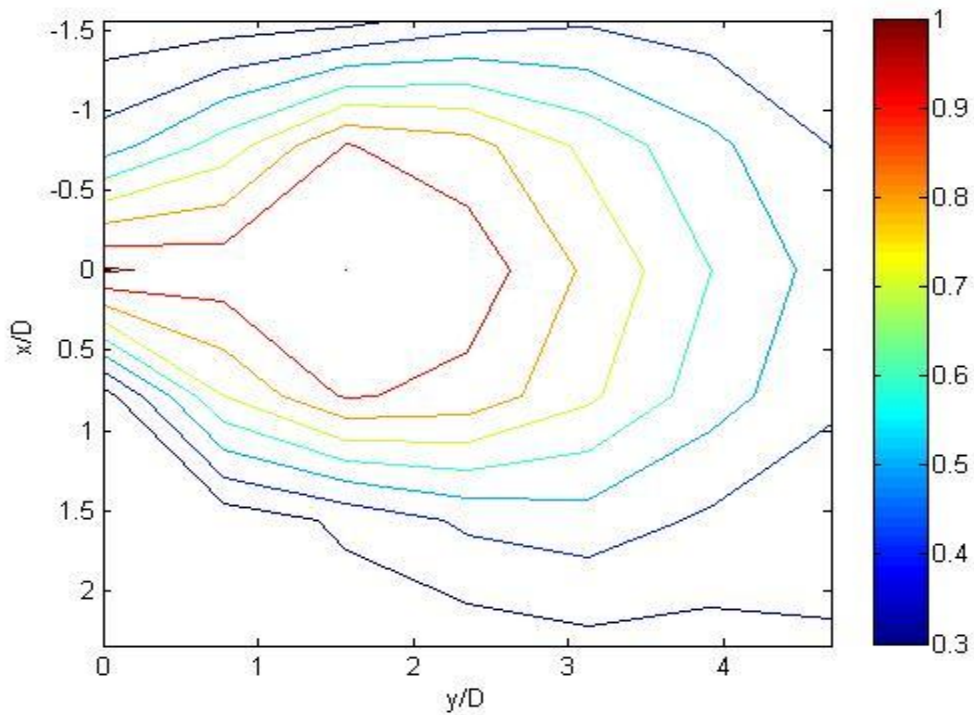


Figure 5.12 Contour plot at first level for ratio 2.95

It is obvious that at this level temperature difference is too high as in the case with ratio 1.97. On the other hand, because of the higher velocity of the jet the highest temperatures are spreading more in the mixed jet. Again in this case, the highest temperature at this level is around the direction of pipe center.

In the following figures thermocouple was positioned at 6.4 mm (one pipe diameter) above the pipe center.

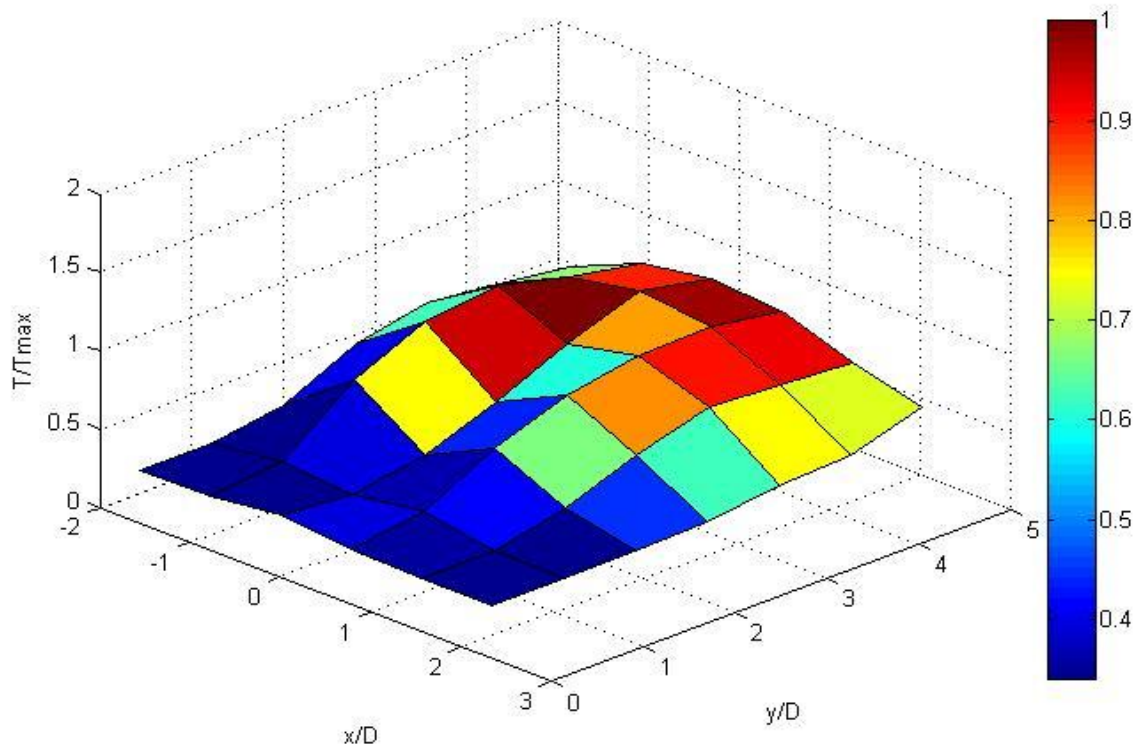


Figure 5.13 3-D plot at second level for ratio 2.95

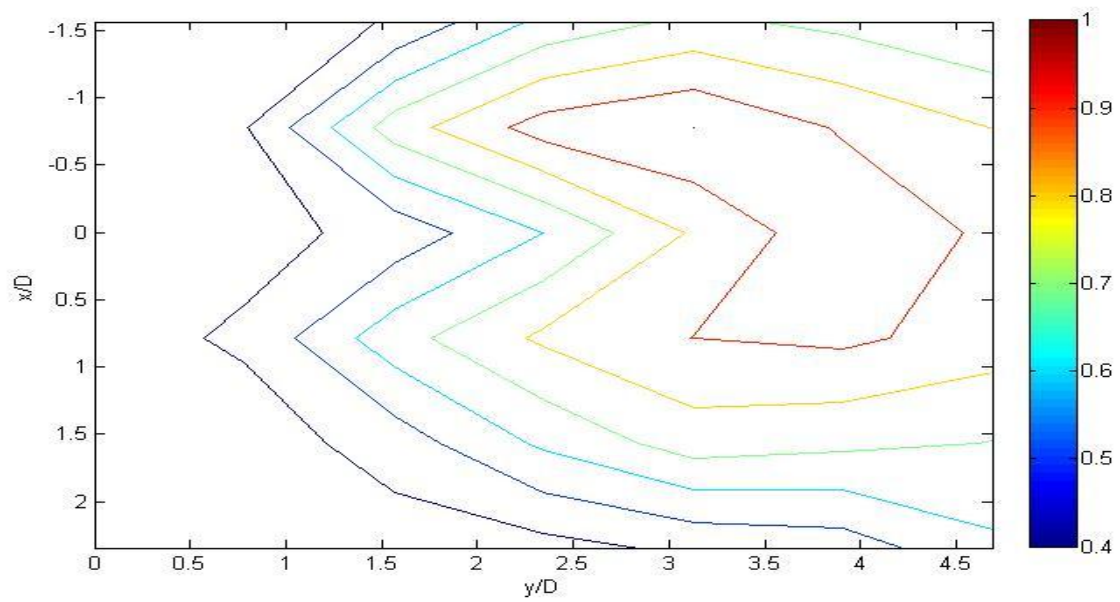


Figure 5.14 Contour plot at second level for ratio 2.95

At this level temperature differences are still high. The highest temperatures are around the direction of pipe center.

In the following figures thermocouple was positioned at 12.8 mm (two pipe diameter) above the pipe center.

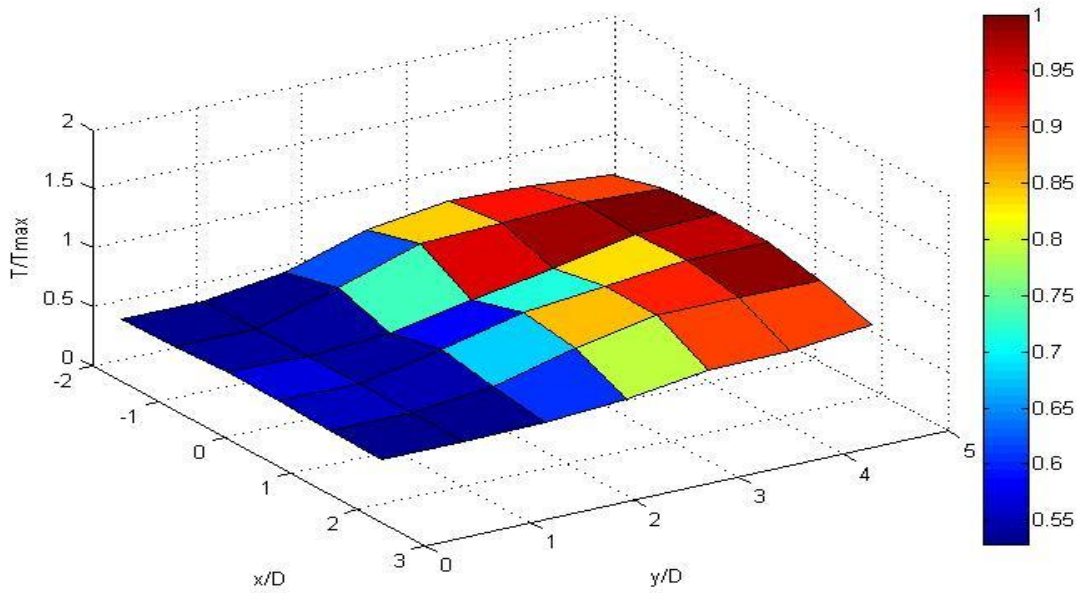


Figure 5.15 3-D plot at third level for ratio 2.95

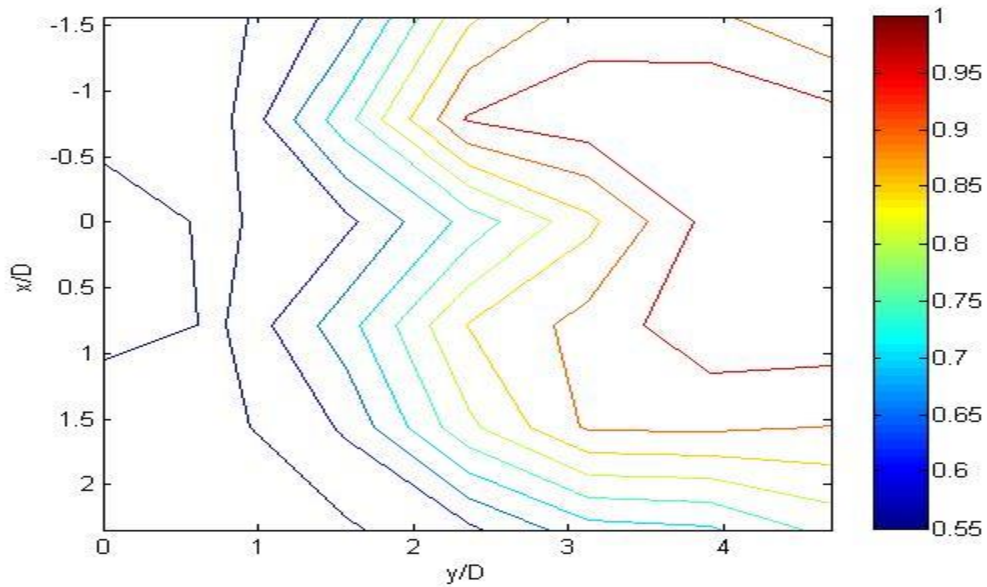


Figure 5.16 Counterplot at third level for ratio 2.95

At this level temperature differences are smaller than the others. Development of mixing is visible. The highest temperature values go closer to the wall that is opposite to the pipe exit.

In the following figures thermocouple was positioned at 32 mm (five pipe diameter) above the pipe center.

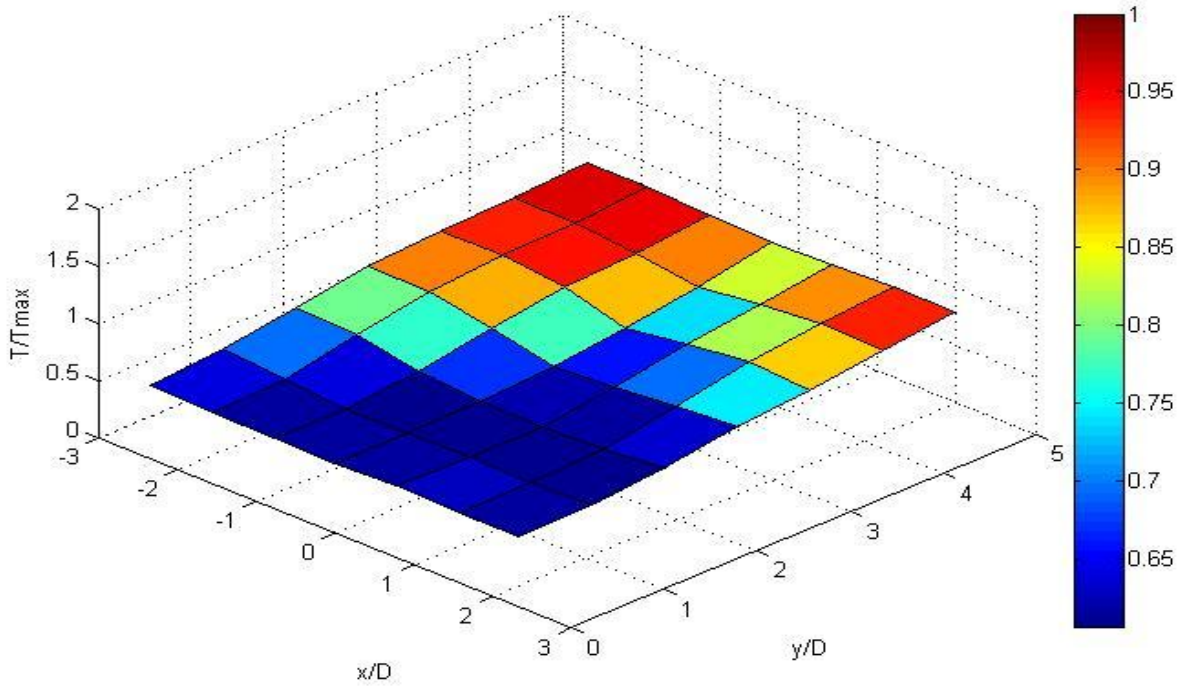


Figure 5.17 3-D plot at fourth level for ratio 2.95

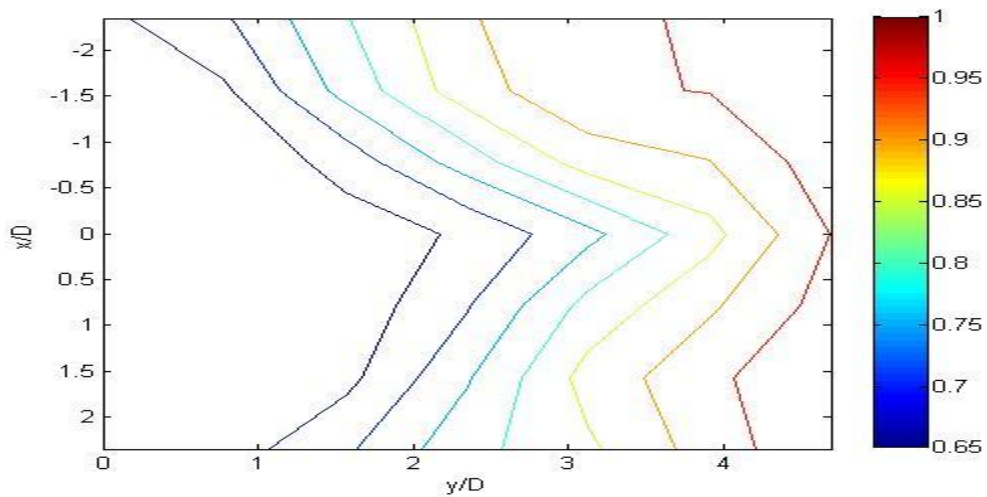


Figure 5.18 Contour plot at fourth level for ratio 2.95

At this level the mixing process is almost completed. Temperature differences decrease rapidly. The highest temperature values divided into two branches which follow the direction of pipe center.

In the following figures thermocouple was positioned at 64 mm (ten pipe diameter) above the pipe center.

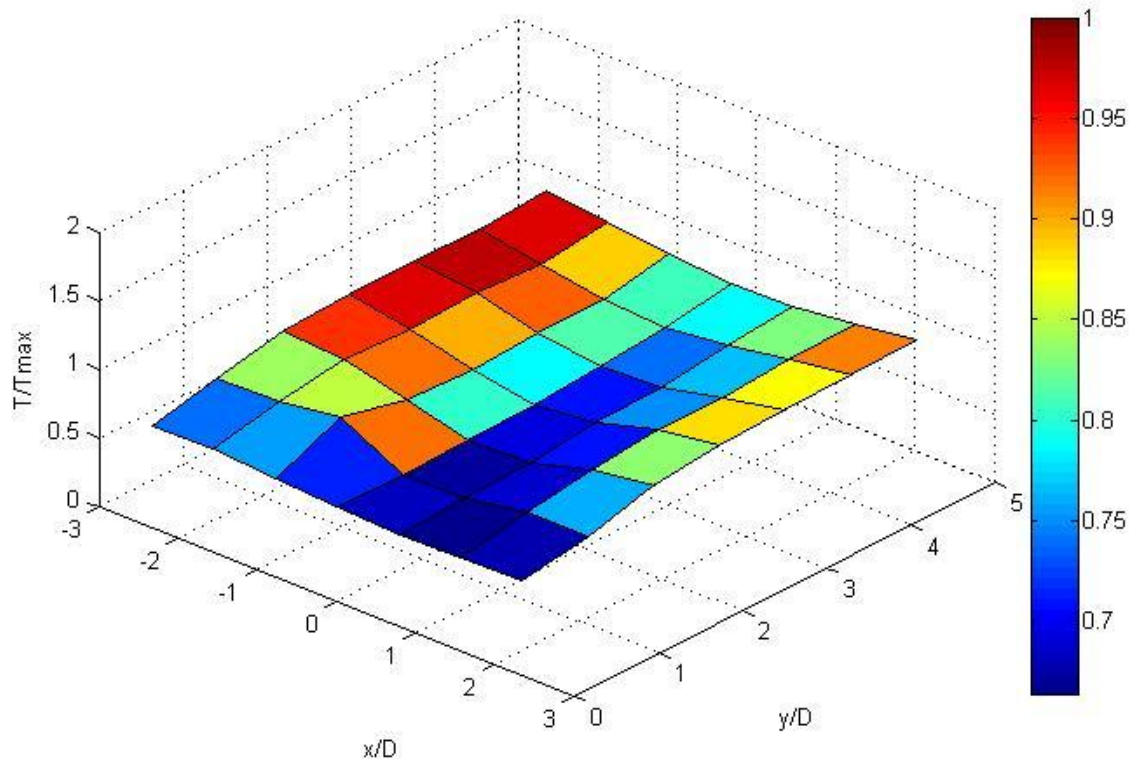


Figure 5.19 3-D plot at final level for ratio 2.95

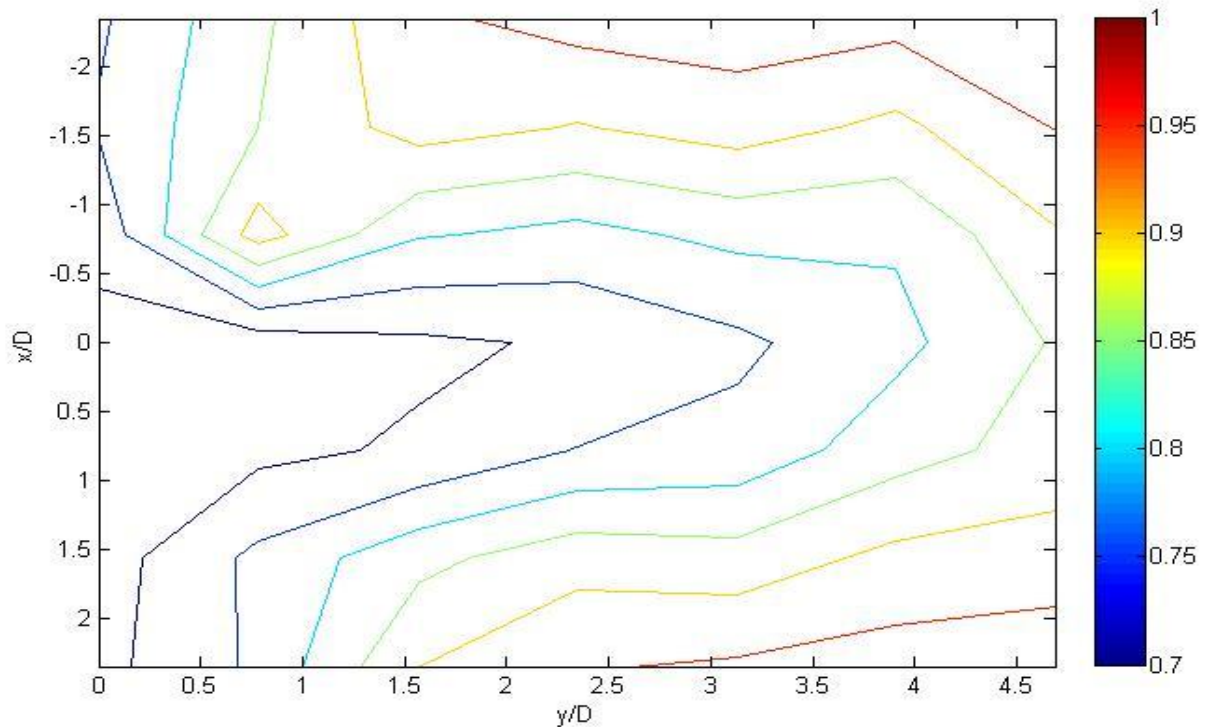


Figure 5.20 Contour plot at final level for ratio 2.95

At this level temperature differences are almost negligible. Since the heated jet hit the opposite wall and came back, in the figures there are two high temperature zones. The lowest temperature values are in the middle of the duct. At this point it can be seen the effect of the ratio on temperature distribution. As it is seen from the figures showed until now, higher velocity ratio gives faster and better mixing.

5.3 Analysis of Data for Ratio 4.95

The same experiment was done with different ratios to observe mixing better. After the experiments for ratio 2.95 done, another experiment with ratio 4.95 was done by following the same procedure.

In the following figures thermocouple was positioned at the same level with pipe center.

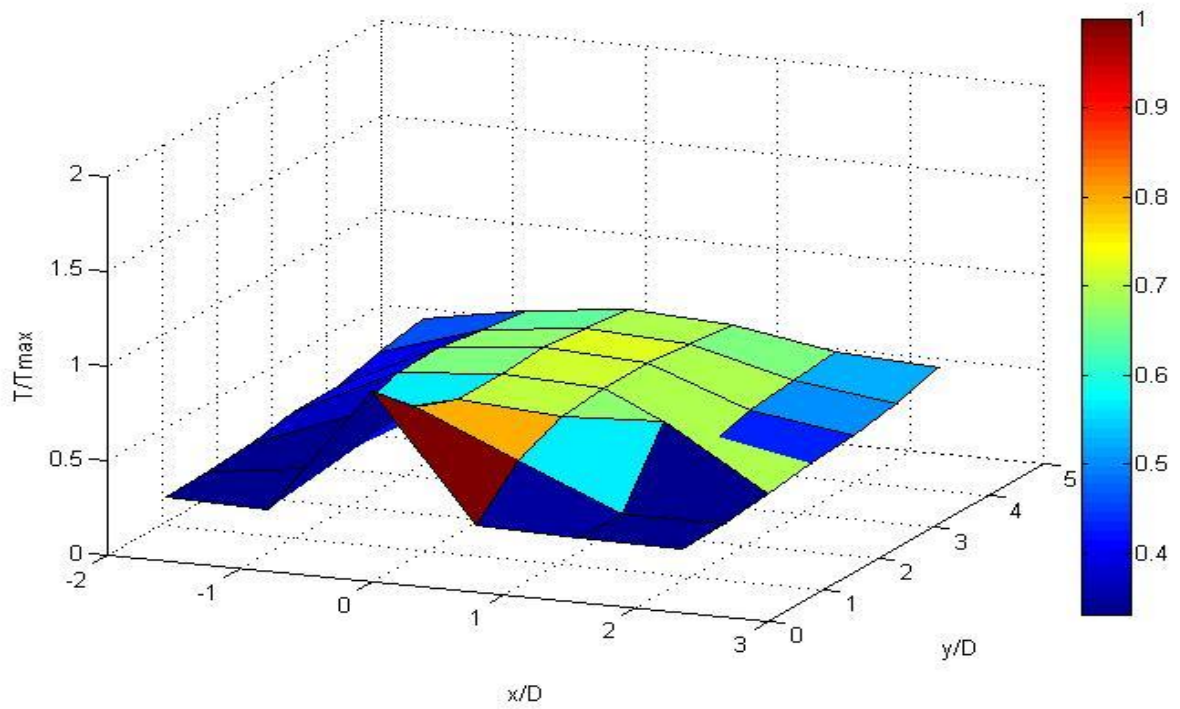


Figure 5.21 3-D plot at first level for ratio 4.95

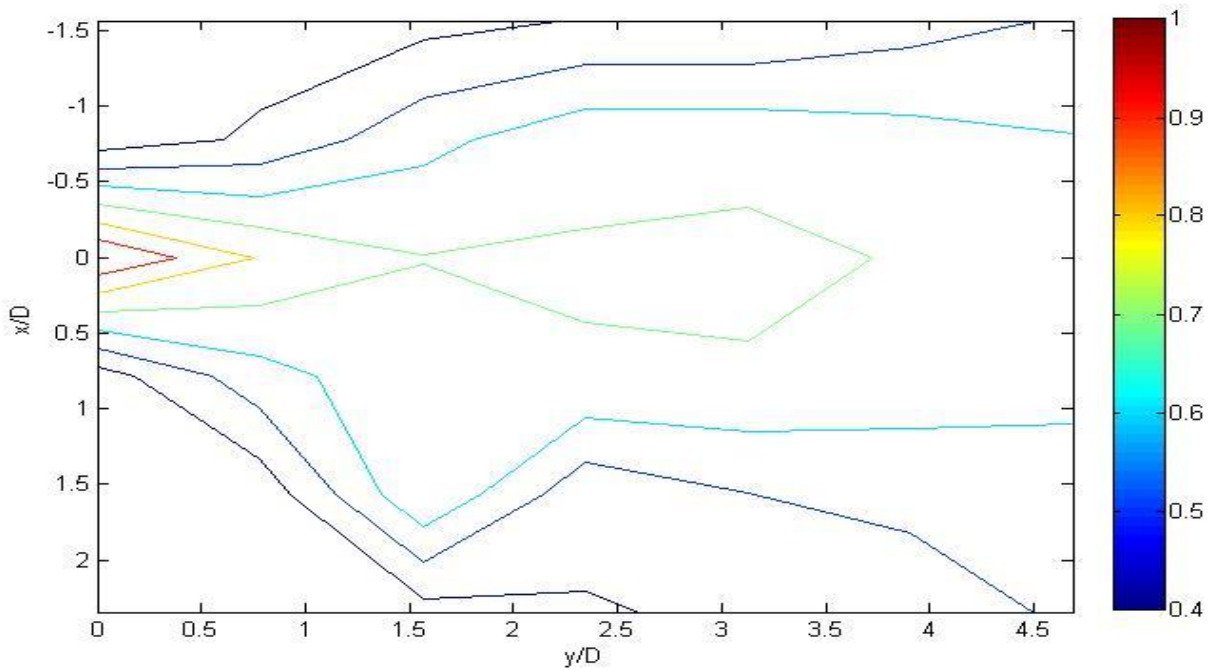


Figure 5.22 Counterplot at first level for ratio 4.95

As it is seen in the figures above, the temperature difference is high. In this case, the highest temperature values spread more than the ones of the ratio 4.95. Mixing just began.

In the following figures thermocouple was positioned at 6.4 mm (one pipe diameter) above the pipe center.

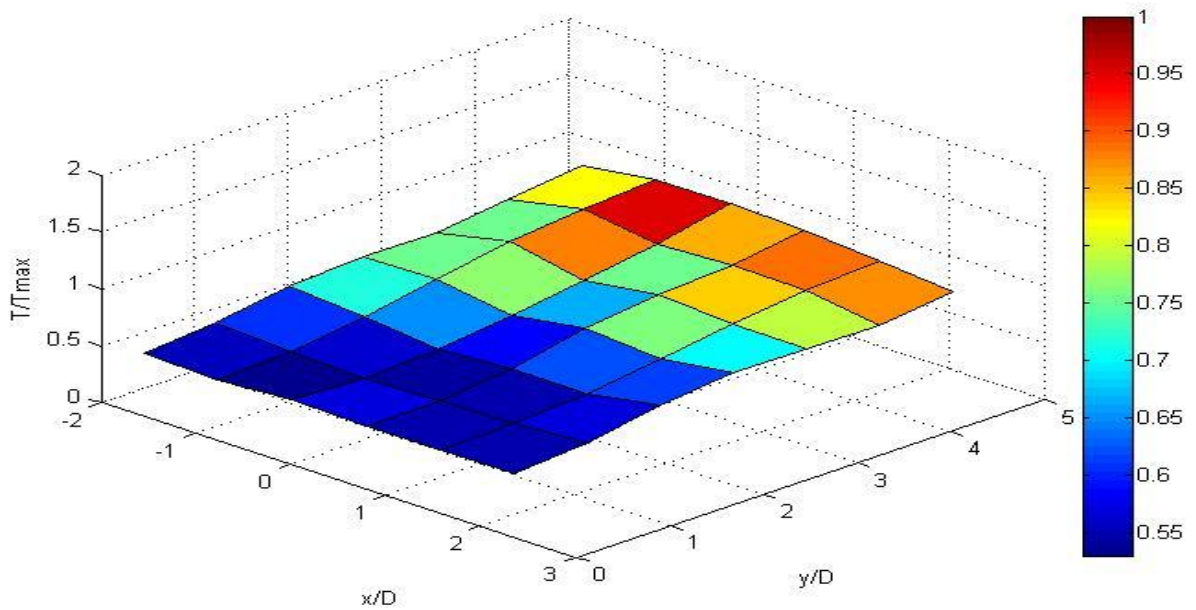


Figure 5.23 3-D plot at second level for ratio 4.95

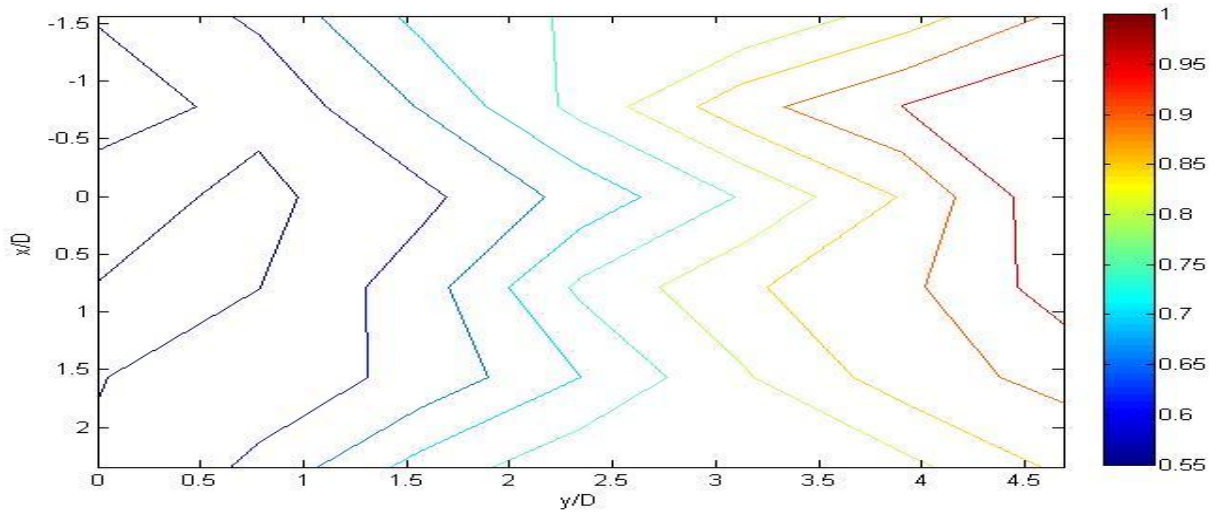


Figure 5.24 Contour plot at second level for ratio 4.95

This time, development of mixing is faster. As it is seen, temperature differences decrease dramatically for ratio 4.95. Temperature distribution looks like in the case of ratio 2.95.

In the following figures thermocouple was positioned at 12.8 mm (two pipe diameter) above the pipe center.

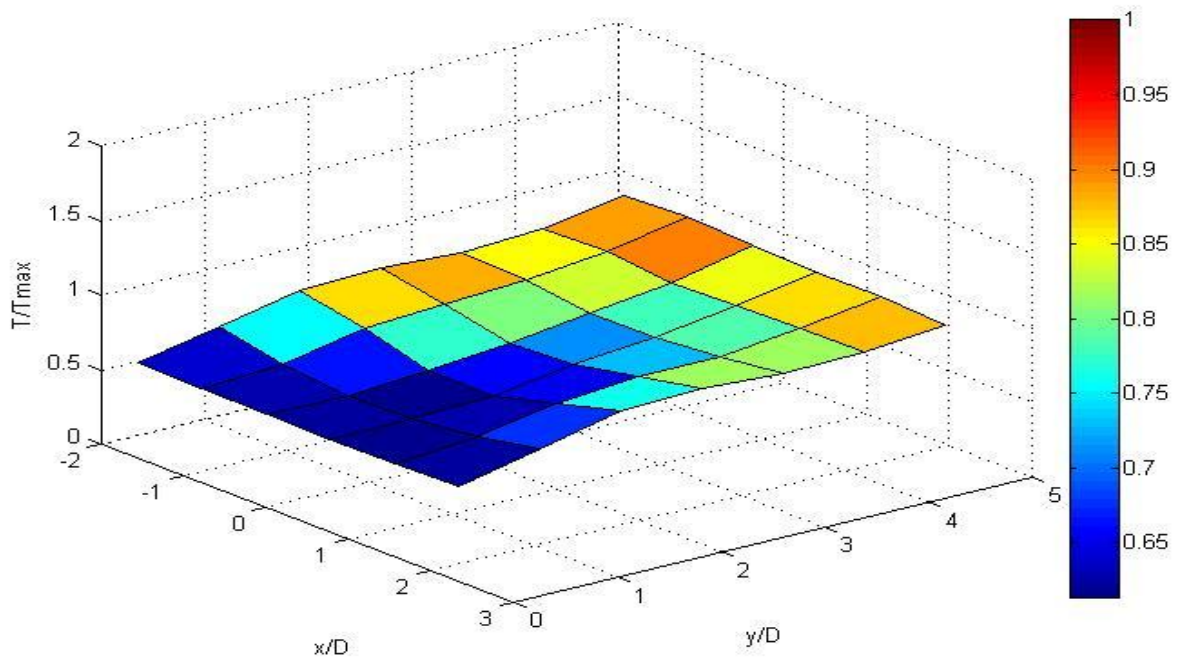


Figure 5.25 3-D plot at third level for ratio 4.95

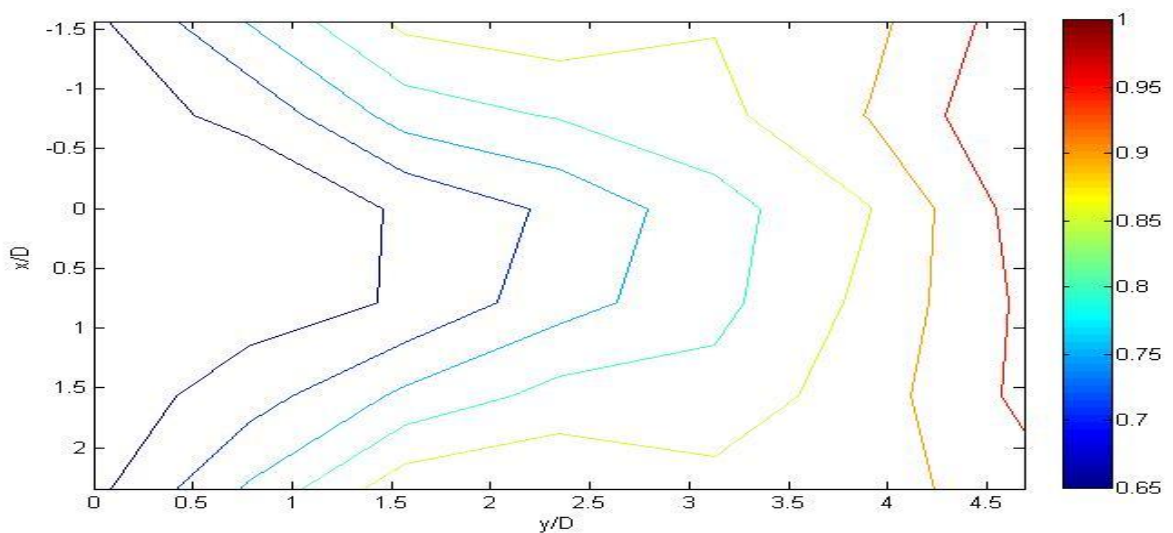


Figure 5.26 Contour plot at third level for ratio 4.95

This time, as it is seen in the figures temperature differences decreases again. Temperature distribution tends to be uniform.

In the following figures thermocouple was positioned at 32 mm (five pipe diameter) above the pipe center.

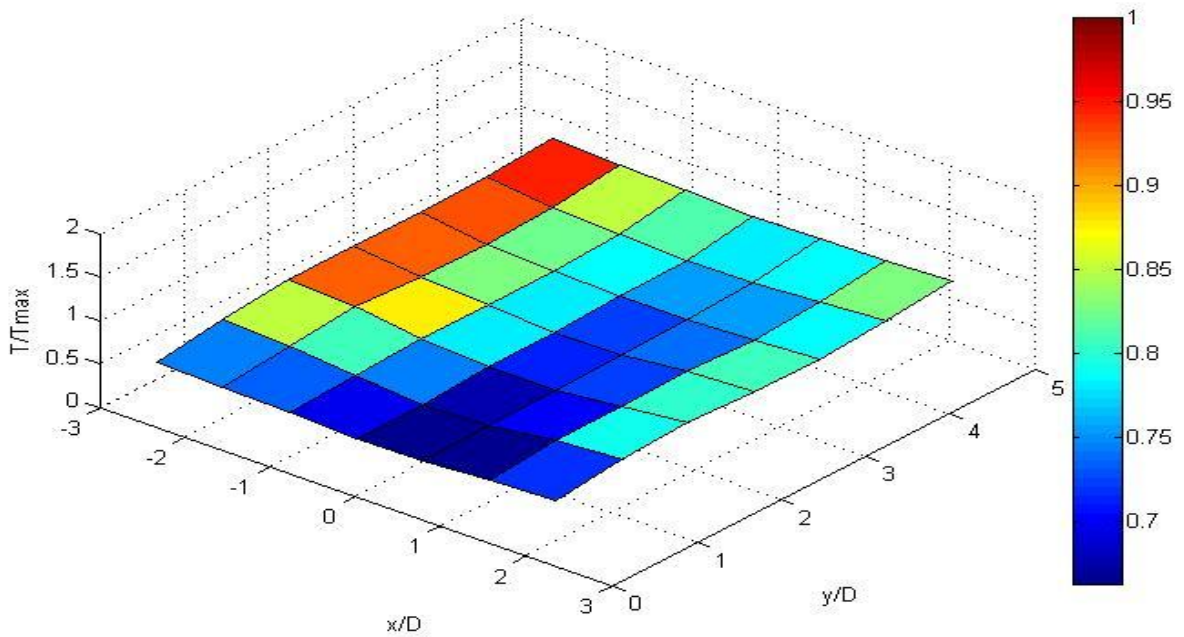


Figure 5.27 3-D plot at fourth level for ratio 4.95

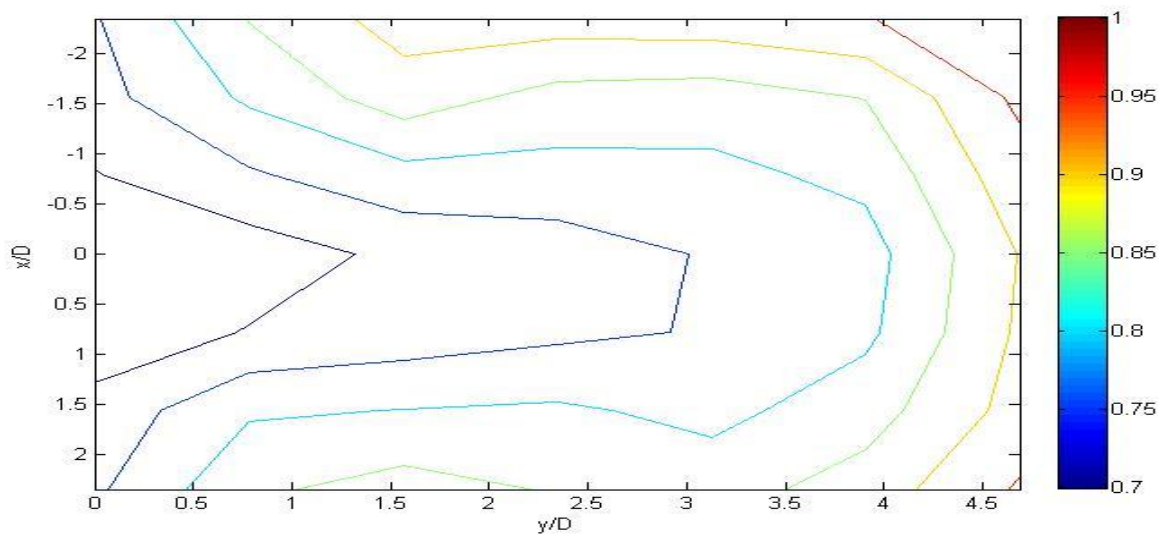


Figure 5.28 Contour plot at fourth level for ratio 4.95

This time temperature distribution is more uniform. Temperature differences are considerably low.

In the following figures thermocouple was positioned at 64 mm (ten pipe diameter) above the pipe center.

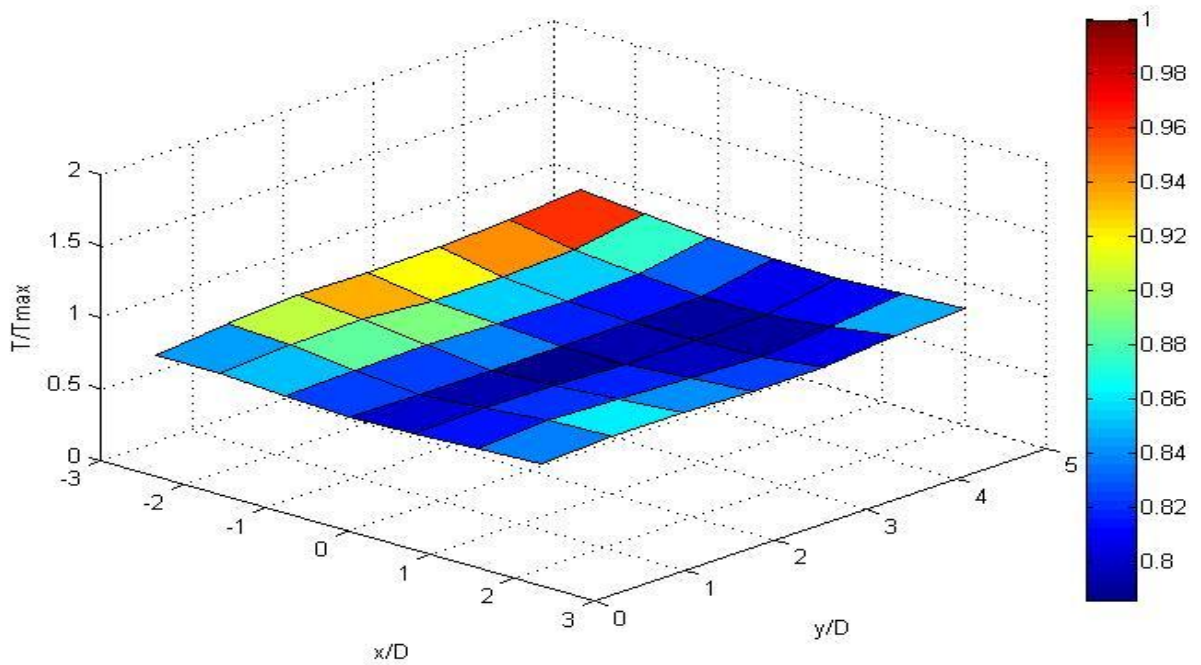


Figure 5.29 3-D plot at final level for ratio 4.95

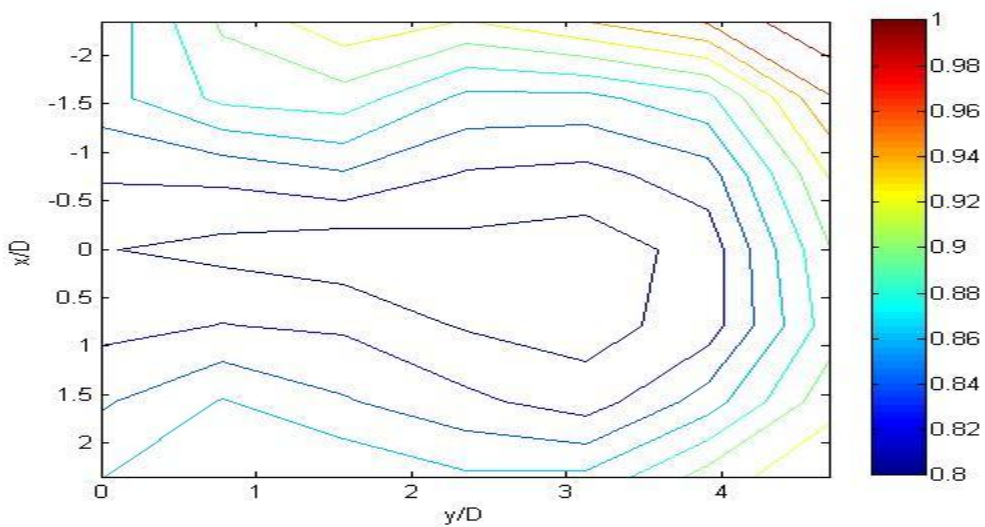


Figure 5.30 Counterplot at final level for ratio 4.95

It can be clearly seen that the temperature distribution is almost uniform. Among all three cases, in this case at the exit section, temperature distribution is the most uniform. Temperature differences are negligibly small.

5.4 Standard Deviation

When number of measurements is high enough, the statistic rules become important. Thus, it is important to look at the standard deviation basically. In the following figures the change in the standard deviation which is an average value over all the measured points versus distance from the mixing section divided by diameter are plotted for each velocity ratio. A non dimensional temperature which was normalized to inlet maximum temperature was used.

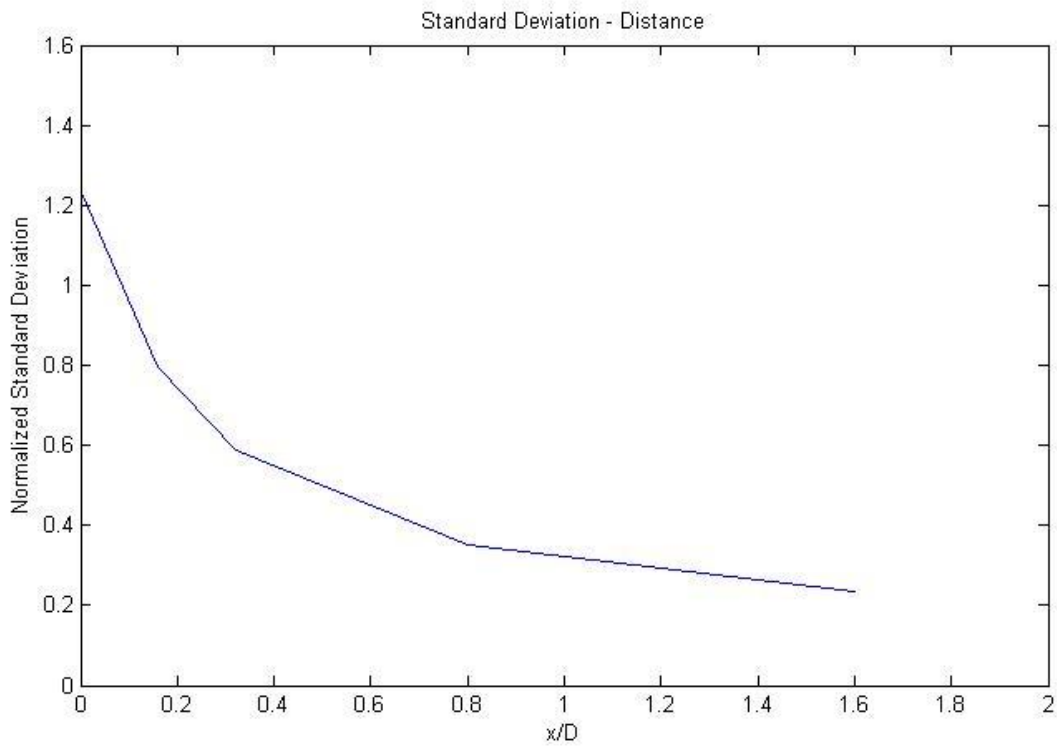


Figure 5.31 Standard deviation change for ratio 1.97

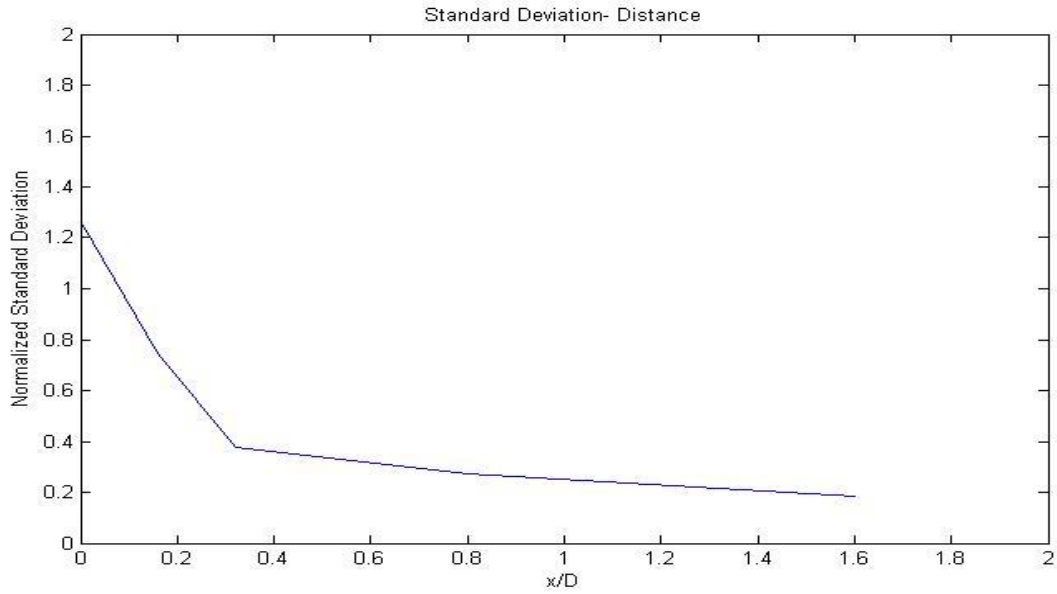


Figure 5.32 Standard deviation change for ratio 2.95

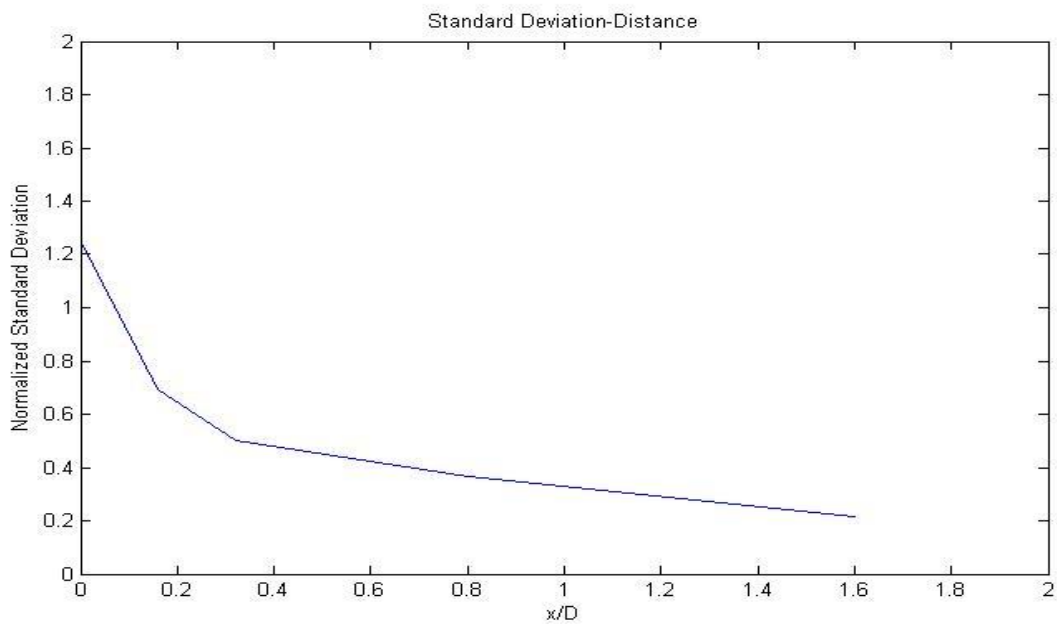


Figure 5.33 Standard deviation change for ratio 4.95

As it is seen in the figures standard deviation of the temperature values decreases for each ratio. The reason of this tendency is that when distance from mixing section increases, the uniformity of temperature distribution increases.

6. CONCLUSION

This study was based on the heated jets in the cross flows. The analysis focused on mixing and interaction of two flows which had different temperatures and mix crossly. In this study a single jet was analyzed by changing flow rate and temperature of it.

The jet was heated by means of a heater which was located just before the cross mixing. In this study, air was chosen for both of the fluids. The flow rate of heated jet was changed and for each case velocity ratios were selected. To select velocity ratios previous experiments were considered and ratios have been directly taken from those. A correction procedure was followed for the air flow meters in the laboratory. After all corrections, the flow rates corresponding each velocity ratios were determined. A thermocouple was placed in the duct and was connected to acquisition devices of computer. By means of controller thermocouple was moved inside the duct to get the temperature values at different points. The distributions of temperature at several sections were measured by means of thermocouple and data was analyzed by means of computer.

The experiments were done in the way described above. Firstly, it was found that if the distance from mixing section increases the mixing process develops. Secondly, the effects of velocity ratios were observed. If the velocity ratio goes higher, the mixing between flows become faster and flows mix better. At the end it was observed that when distance from mixing section increases, the uniformity of temperature distribution increases. Thus, standard deviation lowers with the increase in distance.

REFERENCES

- [1] Margason, Richard J.; and Fearn, Richard: Jet-Wake Characteristics and Their Induced Aerodynamic Effects on V/STOL Aircraft in Transition Flight. Analysis of a Jet in a Subsonic Crosswind, NASA SP-218, 1969.

- [2] Gordier, Robert L.: Studies on Fluid Jets Discharging Normally Into Moving Liquid. Tech. Paper No. 28, Ser. B (Contract Nonr 710(26)), St. Anthony Falls Hydraulic Lab., Univ. of Minnesota, Aug. 1959.

- [3] Margason, Richard J.: The Path of a Jet Directed at Large Angles to a Subsonic Free Stream. NASA TN D-4919, 1968.

- [4] Platten, J. L.; and Keffer, J. F.: Deflected Turbulent Jet Flows. Trans. ASME, Ser. E: J. Appl. Mech., vol. 38, no. 4, Dec. 1971.

- [5] Keffer, J. F.; and Baines, W. D.: The Round Turbulent Jet in a Cross-Wind. J. Fluid Mech., vol. 15, Pt. 4, Apr. 1963.

- [6] Kamotani, Yasuhiro; and Greber, Isaac: Experiments on a Turbulent Jet in a CrossFlow. FTAS/TR- 71-62 (NASA Grant NGR-36-027-008), Case Western Reserve Univ., June 1971.

- [7] Morton, B. R.: On a Momentum-Mass Flux Diagram for Turbulent Jets, Plumes, and Wakes. J. Fluid Mech., vol. 10, pt. 1, Feb. 1961.

- [8] Ricou, F. P.; and Spalding, D. B.: Measurements of Entrainment by Axisymmetrical Turbulent Jets. J. Fluid Mech., vol. 11, Pt. 1, Aug. 1961.

- [9] Campbell, James F.; and Schetz, Joseph A.: Penetration and Mixing of Heated Jets in a Waterway With Application to the Thermal Pollution Problem. AIAA Paper No. 71-524, May 1971.

- [10] Wooler, P. T.; Burghart, G. H.; and Gallagher, J. T.: Pressure Distribution on a Rectangular Wing With a Jet Exhausting Normally Into an Airstream. *J. Aircraft*, vol. 4, no. 6, Nov.-Dec. 1967.
- [11] Hoult, David P.; Fay, James A.; and Forney, Larry J.: A Theory of Plume Rise Compared With Field Observations. *J. Air Pollution Control Assoc.*, vol. 19, no. 8, Aug. 1969.
- [12] Hoult, D. P.; and Weil, J. C.: Turbulent Plume in a Laminar Cross Flow. *Fluid Mech. Lab. Publ. No. 70-8*, Massachusetts Inst. Technol., Oct. 1970.
- [13] Hirst, E. A.: Analysis of Round, Turbulent, Buoyant Jets Discharged to Flowing Stratified Ambients. ORNL-4685, U.S. At. Energy Comm., June 1971.
- [14] James F. Campbell and Joseph A. Schetz Angley Research Center, Analysis of the Injection of a Heated Turbulent Jet into a Cross Flow, 1971.
- [15] D.S. Liscinsky and B. True. United Technologies Research Center , Experimental Investigation of Crossflow Jet Mixing in a Rectangular Duct, 1993.
- [16] Charles Herzfeld, F.G. Brickwedde: Temperature – Its Measurement and Control in Science and Industry, Vol. 3, Part 1, Reinhold, New York, 1962.
- [17] Bulletin 9612, Rev. B: Platinum Resistance Temperature Sensors, Rosemount Engineering Co., 1962.
- [18] Robert P. Benedict: Fundamentals of Temperature, Pressure and Flow Measurements, John Wiley & Sons, Inc., New York, 1969.
- [19] Manual on the Use of Thermocouples in Temperature Measurement, Fourth Edition, Revision of ASTM Special Publication 470B, Philadelphia, PA., 1993.

- [20] [21] Temperature-Electromotive Force Reference Functions and Tables for the Letter-Designated Thermocouple Types Based on the ITS-90, NIST Monograph 175, National Institute of Standards and Technology, Washington, D.C., 1993.
- [22] R.P. Reed: Thermoelectric Thermometry. A Functional Model, from Temperature - Its Measurement and Control in Science and Industry, Vol. 5, American Institute of Physics, N.Y. 1982.